

1 **Evaluation of biogeochemical models performance and recommendation on**
2 **observing system design using an unsupervised machine learning**
3 **algorithm, BGC-Argo floats and assessment metrics**

4

5

6 Alexandre Mignot¹, Hervé Claustre^{2,3}, Gianpiero Cossarini⁴, Fabrizio D’Ortenzio^{2,3}, Elodie
7 Gutknecht¹, Julien Lamouroux¹, Paolo Lazzari⁴, Coralie Perruche¹, Stefano Salon⁴, Raphaëlle
8 Sauzède³, Vincent Taillandier^{2,3}, Anna Teruzzi⁴

9

10 ¹Mercator Océan International, Toulouse, France

11 ²Laboratoire d’Océanographie de Villefranche-sur-Mer, Villefranche-sur-Mer, CNRS and
12 Sorbonne Université, 06230 Villefranche-sur-Mer, France

13 ³Institut de la Mer de Villefranche, CNRS and Sorbonne Université, 06230 Villefranche-sur-
14 Mer, France

15 ⁴National Institute of Oceanography and Applied Geophysics - OGS, Trieste, Italy

16

17

18 Numerical models of ocean biogeochemistry are becoming major tools to detect and predict
19 the impact of climate change on marine resources and monitor ocean health. However, the
20 assessment of biogeochemical models is becoming increasingly challenging due to the
21 continuous improvement in model structure and spatial resolution. Here, we propose a new
22 method to inform about the model predictive skill in a concise way. The method is based on
23 the conjoint use of a K-means clustering technique -- an unsupervised machine learning
24 algorithm, assessment metrics and BGC-Argo observations. The K-means algorithm and the
25 assessment metrics reduce the number of model data points to be evaluated. The metrics
26 evaluate either the model state accuracy or the skill of the model in capturing emergent
27 properties, such as the Deep Chlorophyll Maximums and Oxygen Minimum Zones. The use
28 of BGC-Argo observations as the single evaluation data set ensure the accuracy of the data as
29 it is an homogenous data set with strict sampling methodologies and data quality control
30 procedures. The method is applied to the Copernicus Marine Service global forecasting
31 system. The model performance is evaluated using the model efficiency statistical score that
32 compare the model-observations misfit with the variability of the observations, and thus
33 objectively quantifies whether the model outperforms the BGC-Argo climatology. We show

1 that, overall, the model surpass the BGC-Argo climatology in predicting pH, dissolved
2 inorganic carbon, alkalinity and oxygen in the mesopelagic and the mixed layers, nitrate,
3 silicate and phosphate in the mesopelagic layer. We provide suggestions to reduce the model-
4 data misfit for phosphate, silicate, pH and the partial pressure of CO₂ in the mixed layer,
5 chlorophyll-a related and particulate organic carbon metrics, and Oxygen Minimum Zones.
6 The method proposed here is also helpful to inform about the design of the BGC-Argo
7 network. In particular, the regions where BGC-Argo observations should be enhanced to
8 improve the model accuracy through the assimilation of BGC-Argo data or process-oriented
9 assessment studies. We strongly recommend to enhance the Arctic region, which is critically
10 under sampled and where the model is constantly outperformed by the BGC-Argo
11 climatology. BGC-Argo observations should also be reinforced in the Equatorial region and
12 in the Southern Oceans, two regions where the model predictions barely exceed the BGC-
13 Argo climatology. Our results illustrate how the synergic use of modeling and BGC-Argo
14 data can both inform about the performance of models and the design of observing systems.

15
16

17 **1. Introduction**

18

19 Since pre-industrial times, the ocean has taken ~26 % of the total anthropogenic CO₂
20 emission (Friedlingstein et al., 2022) leading to dramatic change in the ocean's
21 biogeochemical (BGC) cycles, such as ocean acidification (Iida et al., 2020). Moreover,
22 deoxygenation (Breitburg et al., 2018) and change in the biological carbon pump are now
23 manifesting globally (Capuzzo et al., 2018; Osman et al., 2019; Roxy et al., 2016). Together
24 with plastic pollution (Eriksen et al., 2014) and an increase in fisheries pressure (Crowder et
25 al., 2008), major changes are therefore occurring in marine ecosystems at the global scale. In
26 order to contextualize monitoring of ongoing changes, derive climate projections and develop
27 better mitigation strategies, realistic numerical simulations of the oceans' BGC state are
28 required.

29

30 Numerical models of ocean biogeochemistry represent a prime tool to address these issues
31 because they produce three dimensional estimates of a large number of chemical and
32 biological variables that are dynamically consistent with the ocean circulation (Fennel et al.,
33 2019). They can assess past and current states of the BGC ocean, produce short-term to

1 seasonal forecasts as well as climate projections. However, these models are far from being
2 flawless, mostly because there are still huge knowledge gaps in the understanding of key
3 BGC processes and, as a result, the mathematical functions that describe BGC fluxes, and
4 ecosystems dynamics are too simplistic (Schartau et al., 2017). For instance, most models do
5 not include a radiative component for the penetration of solar radiation in the ocean. It has
6 been nevertheless shown that coupling such a component with a BGC model improves the
7 representation of the dynamics of phytoplankton in the lower euphotic zone (Dutkiewicz et
8 al., 2015). Additionally, the parameterisation of the mathematical functions generally results
9 from laboratory experiments on a few representative species and may not be suitable for
10 extrapolation to ocean simulations that need to represent the large range of organisms present
11 in oceanic ecosystems (Schartau et al., 2017; Ward et al., 2010). Furthermore, the assimilation
12 of physical data in coupled physical-BGC models that improves the physical ocean state can
13 paradoxically degrade the simulation of the BGC state of the ocean (Fennel et al., 2019; Park
14 et al., 2018; Gasparin et al., 2021). A rigorous assessment of BGC models is thus essential to
15 test their predictive skills and ability to reproduce BGC processes and estimate confidence
16 intervals on model predictions (Doney et al., 2009; Stow et al., 2009).

17

18 However, the evaluation of BGC models is limited by the availability of data. It relies
19 principally on a combination of different data sets from satellite (such as chlorophyll-*a*
20 concentrations), cruises observations, permanent oceanic stations from large databases such
21 as the WOD. (e.g., Doney et al., 2009; Dutkiewicz et al., 2015; Lazzari et al., 2012, 2016;
22 Lynch et al., 2009; Séférian et al., 2013; Stow et al., 2009). All these datasets have neither a
23 sufficient vertical or temporal resolution, nor a synoptic view, nor provide all variables
24 necessary to evaluate how models represent climate-relevant processes such as the air-sea
25 CO₂ fluxes, the biological carbon pump, ocean acidification or deoxygenation.

26

27 In 2016, the Biogeochemical-Argo (BGC-Argo) program was launched with the goal to
28 operate a global array of 1000 BGC-Argo floats equipped with oxygen (O₂), chlorophyll *a*
29 (Chl*a*) and nitrate (NO₃) concentrations, particulate backscattering (b_{bp}), pH and downwelling
30 irradiance sensors (Biogeochemical-Argo Planning Group, 2016; Claustre et al., 2020).

31 Although the planned number of 1000 floats has not been reached yet, the BGC-Argo
32 program has already provided a large number of quality-controlled vertical profiles of O₂,
33 Chl*a*, NO₃, b_{bp}, and pH (Fig. 1). With respect to O₂, Chl*a*, NO₃, and b_{bp}, the North Atlantic
34 and the Southern Ocean are reasonably well sampled whereas pH is well sampled only in the

1 Southern Ocean. At the regional scale, the Mediterranean Sea is also fairly well sampled by
2 BGC-Argo floats (Salon et al., 2019; Terzić et al., 2019). However, there are still large
3 under-sampled areas like the Arctic ocean, subtropical gyres and the sub-polar North Pacific.
4 Thanks to machine learning based methods (Bittig et al., 2018; Sauzède et al., 2017), floats
5 equipped with O₂ sensors can be additionally used to derive vertical profiles of NO₃,
6 phosphate (PO₄), silicate (Si), alkalinity (Alk), dissolved inorganic carbon (DIC), pH and
7 pCO₂.

8
9 The BGC-Argo data set represents a significant improvement for the assessment of models
10 comparing to large databases such as the World Ocean Database (WOD) (Boyer et al., 2013)
11 or the Copernicus Marine Service in situ dataset (European Union-Copernicus Marine
12 Service, 2015). Large databases are composed of data collected from various instrument types
13 with heterogenous data sampling methodologies. Therefore, for a given variable, the accuracy
14 numbers are not the same and change depending on the instrument type (European Union-
15 Copernicus Marine Service, 2019). Consequently, this affects the overall accuracy over time
16 due to the changing proportion of instrument types over the years. On the other hand, the
17 BGC-Argo data set is an homogenous data set with strict and uniform sampling
18 methodologies and data Quality-Control (QC) procedures. As a result, the BGC-Argo data set
19 have a satisfactory level of accuracy, which remains stable over time (Johnson et al., 2017;
20 Mignot et al., 2019). Moreover, the number of quality-controlled observations collected every
21 year by the BGC-Argo fleet is now greater than any other data set (Claustre et al., 2020).
22 Using the BGC-Argo dataset as the single evaluation data set is therefore a way to ensure
23 consistent accuracy.

24
25 The BGC-Argo floats provide multivariate observations at high vertical and temporal
26 resolutions and for long periods of time providing nearly continuous time series of the vertical
27 distribution of several biogeochemical variables. This is not possible with discrete, univariate
28 vertical samplings provided by cruise cast *in situ* measurements or from climatological values
29 derived from the WOA. All these specificities overcome the limitations of the previous
30 datasets, especially with respect to their univariate nature, as well as their limited vertical and
31 temporal resolution. This opens new perspectives for the evaluation of BGC
32 models(Gutknecht et al., 2019; Salon et al., 2019; Terzić et al., 2019).

33

1 The development of BGC models as well as the continuous increase in spatial and vertical
2 resolutions has reached the point where the volume of model outputs has dramatically
3 increase. Simplification techniques are therefore required to provide decipherable information
4 on model predictive skill. Allen et al. (2007) proposed a methodology for reducing the spatial
5 dimensions in model assessment exercises, thereby providing concise information about the
6 model performance. They use an unsupervised learning algorithm to classify the Southern
7 North Sea into 5 coherent BGC regions based on modelled time series of temperature, NO₃,
8 NO₃, and Si concentrations. They then evaluated the predictive capabilities of the model in
9 each BGC region (instead of at each grid point), thus greatly reducing the number of points to
10 be validated. An additional method for reducing the dimensions of model-data comparison is
11 the use of assessment metrics (Hipsey et al., 2020; Russell et al., 2018). In particular, metrics
12 such as depth-averaged state variables (e.g., mixed layer averaged Chl_a, NO₃, O₂, etc...),
13 mass fluxes and process rates validation (e.g., primary production or division rates), or
14 emergent properties validation [e.g., Deep Chlorophyll Maximum (DCM), or Oxygen
15 Minimum Zone [OMZ]] are particularly useful to reduce the number of model's vertical
16 layers to be compared with the observations.

17
18 The objectives of the present study are twofold. Our first aim is to propose a methodology
19 that uses the BGC-Argo data set, an unsupervised learning algorithm and assessment metrics
20 to simplify marine BGC model-data comparisons, and thus inform, in a concise way, about
21 model performance. The second objective is to use this methodology to also identify ocean
22 regions where the model-observations misfit is larger than the variability of the BGC-Argo
23 data and thus inform the BGC-Argo observing system of regions that should be better
24 sampled. The first step of the method consists in defining 23 assessment metrics that are used
25 both to construct the BGC regions and then to compare the model outputs with the BGC-Argo
26 data. Second, following the approach of Allen et al. (Allen et al., 2007), we use an
27 unsupervised learning algorithm, here a K-means clustering technique, to classify the global
28 ocean into 8 coherent BGC regions based on the climatological modelled time series of the 23
29 assessments metrics. In the last step, the skill of the model in predicting the assessment
30 metrics is evaluated in each BGC-region, using the model efficiency statistical score. Unlike
31 other statistical metrics such the correlation coefficient, the bias or the root mean square
32 difference, that does not quantifies objectively whether the model performance is acceptable
33 or not; the model efficiency calculates whether the model outperforms an observational
34 climatology (Fennel et al., 2022). Finally, the method is implemented using the Copernicus

1 Marine Service global BGC forecasting system (European Union-Copernicus Marine Service,
2 2019).

3

4 The paper is organised as follows: section 2 presents the data sets used in the study. In section
5 3, we define the assessment metrics and we detail the K-means algorithm as well as the model
6 efficiency statistical score. In section 4, we presents and discuss the results. Finally, section 5
7 concludes the study.

8

9

2. Data

10

11

a. BGC-Argo floats observations

12

13 The float data were downloaded from the Argo Coriolis Global Data Assembly Centre in
14 France (<ftp://ftp.ifremer.fr/argo>). The CTD and trajectory data were quality controlled using
15 the standard Argo protocol (Wong et al., 2015). The raw BGC signals were transformed to
16 biogeochemical variables (i.e., O₂, Chl_a, NO₃, b_{bp}, and pH) and quality-controlled according
17 to international BGC-Argo protocols (Johnson et al., 2018b, a; Schmechtig et al., 2015, 2018;
18 Thierry et al., 2018; Thierry and Bittig, 2018).

19

20 In the Argo data-system, the data are available in three data modes: “Real-Time”, ”Adjusted”
21 and ”Delayed” (Bittig et al., 2019). In the “Real-time” mode, the raw data are converted into
22 state variables and an automatic quality-control is applied to “flag” gross outliers. In the
23 “Adjusted” mode, the “Real-time” data receive a calibration adjustment in an automated
24 manner. In the “Delayed” mode, the “Adjusted” data are adjusted and validated by a scientific
25 expert. While the “Real-Time” and “Adjusted” data are considered acceptable for operational
26 application (data assimilation), the “Delayed” mode” is designed for scientific exploitation
27 and represent the highest quality of data with the ultimate goal, when time-series with
28 sufficient duration will have been acquired, to possibly extract climate-related trends
29 (Bojinski et al., 2014). However, for some variables, only a limited fraction of data is
30 accessible in “Delayed-Mode”. Consequently, for each variable, we selected the highest level
31 of data modes, where at least 80 % of the data are available (see Table 1). Note that this
32 criterion does not apply to O₂, where only delayed mode data were selected in order to
33 generate the pseudo-observations from CANYON-B neural network (see after). We removed

1 data with missing location or time information and flagged as “Bad data” (flag =4).
 2 Depending on the parameter and the associated data mode, we also excluded data flagged as
 3 “potentially bad data” (flag=3) (see Table 1).

4
 5 Particulate Organic Carbon (POC) concentrations were derived from b_{bp} observations. First,
 6 three consecutive low-pass filters were applied on the vertical profiles of b_{bp} to remove
 7 spikes (Briggs et al., 2011): a 2-point running median followed by a 5-point running
 8 minimum and 5-point running maximum. Then, the filtered b_{bp} profiles were converted into
 9 POC (mgC m^{-3}) using a simplified version of the empirical POC/ b_{bp} algorithm developed by
 10 Gali et al. (2022), i.e., for depths larger than the mixed layer depth (MLD):

$$\frac{POC}{b_{bp}} = c + a \cdot e^{-0.001 \cdot b \cdot (z - MLD)}, \quad (1)$$

$$z > MLD,$$

11
 12
 13
 14
 15 where c is a constant deep value and, b , the slope of the exponential decrease, sets to 12010
 16 $\text{mgC m}^{-3} \text{ m}$ and 6.57, respectively, as proposed by Gali et al. (2022). The global coefficient a ,
 17 is set to 37990 $\text{mgC m}^{-3} \text{ m}$ to be consistent with a relationship, developed for global surface
 18 applications (i.e., $POC = 38687.27 \cdot b_{bp}^{0.95}$) (European Union-Copernicus Marine Service,
 19 2020). This relationship is based on a global database of *in situ* POC and satellite b_{bp} (Evers-
 20 King et al., 2017). In the mixed layer (ML), z is fixed at MLD, and the Eq. (1) simplifies to

$$\frac{POC}{b_{bp}} = c + a, \quad (2)$$

$$z \leq MLD.$$

21
 22
 23
 24
 25 Finally, we complemented the existing BGC-Argo dataset with pseudo-observations of NO_3 ,
 26 PO_4 , Si, Alk, and DIC concentrations as well as pH and pCO_2 using the CANYON-B neural
 27 network (Bittig et al., 2018). CANYON-B estimates vertical profiles of nutrients as well as
 28 the carbonate system variables from concomitant measurements of float pressure,
 29 temperature, salinity, and O_2 qualified in “Delayed“ mode together with the associated
 30 geolocalization and date of sampling. CANYON-B was trained and validated using the
 31 GLODAPv2 data set (Key et al., 2015). The CANYON-B estimates of NO_3 and pH were
 32 merged with measured values on the rationale that CANYON-B estimates have RMS errors (

1 $\text{NO}_3 = 0.7 \mu\text{mol kg}^{-1}$, $\text{pH} = 0.013$) (Bittig et al., 2018) that are of the same order of
2 magnitude as those of the BGC-Argo observations errors ($\text{NO}_3 = 0.5 \mu\text{mol kg}^{-1}$, $\text{pH} = 0.07$)
3 (Mignot et al., 2019; Johnson et al., 2017) .
4

5 Finally, we verified that the RMS errors of BGC-Argo data (both measured and from
6 CANYON-B estimates) are lower than the RMS difference between the model and BGC-
7 Argo data, so that the comparison of simulated properties with the BGC-Argo data leads to a
8 meaningful evaluation of the model performance. We believe it is reasonable to draw
9 conclusions on the model uncertainty from BGC-Argo data as long as the BGC-Argo errors
10 are much lower than the model-observations RMS difference.
11

12

13 **b. Copernicus Marine Service global BGC Model**

14

15 The global model simulation used in this study (see Appendix A.1) originates from the Global
16 Ocean hydrodynamic-biogeochemical model implemented and operated by the Global
17 Monitoring and Forecasting Center of the EU, the Copernicus Marine Service. It is based on
18 the coupled NEMO–PISCES model and is constrained by the assimilation of satellite *Chla*
19 concentrations. The BGC model is forced offline by daily fields of ocean, sea ice and
20 atmosphere. The ocean and sea ice forcing come from Mercator Ocean global high-resolution
21 ocean model (Lellouche et al., 2018) that assimilates along-track altimeter data, satellite Sea
22 Surface Temperature and Sea-Ice Concentration, and *in situ* temperature and salinity vertical
23 profiles. The BGC model has a $1/4^\circ$ horizontal resolution, 50 vertical levels (with 22 levels in
24 the upper 100 m, the vertical resolution is 1 m near the surface and decreases to 450 m
25 resolution near the bottom). It produces daily outputs of *Chla*, NO_3 , PO_4 , Si, O_2 , pH, DIC and
26 Alk, and weekly outputs of POC (resampled offline from weekly to daily frequency through
27 constant interpolation) from 2009 to 2020. Note that the method of linear resampling, while
28 artificially increasing the number of data, could potentially bias the statistical results,
29 especially in regions with poor data coverage. Then, following the approach of Galí et al.
30 (2022), the POC simulated by the model corresponds to the sum of the two sizes classes of
31 phytoplankton, the small detrital particles and microzooplankton modelled by PISCES. This
32 particular combination of phytoplanktonic and non-phytoplanktonic organisms has been
33 shown to match the small POC observed by the floats (Galí et al., 2021). The partial pressures

1 of CO₂ values are extrapolated in the mixed layer from the surface value estimated by the
2 model. The Black Sea was not considered in the present analysis because the model solutions
3 are of poor qualities. Finally, the daily model outputs were collocated in time and space
4 closest to the BGC-Argo floats positions, and they were interpolated to the sampling depth of
5 the float observations. The characteristics of the model are further detailed in the appendix.

6 7 **3. Methods**

8 **a. Assessment metrics**

9
10 In this section, we present 23 metrics used for the clustering of the ocean and for the
11 assessment of the model simulation with BGC-Argo data. The metrics are associated with the
12 carbonate chemistry, the biological carbon pump, and oxygen levels. Most of the metrics
13 evaluate the model state accuracy through the comparison of simulated state variables with
14 BGC-Argo observations depth-averaged in the mixed (hereafter indicated with the subscript
15 *mixed*) and mesopelagic (hereafter indicated with the subscript *meso*) layers. This two-layer
16 comparison between model and BGC-Argo data provides an indirect evaluation of the key
17 mesopelagic processes and fluxes associated with the carbonate chemistry, biological carbon
18 pump and oxygen levels in the mixed, and mesopelagic layers. In addition, some of the
19 metrics assess the skill of the model in capturing emergent properties, such as the nitracline,
20 the DCM and the OMZs. The metrics are described below and summarized in Table 2. The
21 definition of the metrics is the same for the model and the BGC-Argo data. The MLD is
22 computed, following De Boyer et al. (2004), as the depth at which the change in potential
23 density from its value at 10 m exceeded 0.03 kg m⁻³. The mesopelagic layer is defined as the
24 layer between the MLD and 1000m. For simplicity, we use a simplified definition of the
25 mesopelagic layer proposed by Dall' Olmo and Mork (2014). In their study, this layer is
26 comprised between the deepest of the euphotic layer depth and the MLD, and 1000 m. Given
27 the importance of the MLD in the calculation of the metrics, we verified that the MLD is
28 correctly represented in the model -- the overall mean square difference between the model
29 and the data is equal to ~30% of the overall variance of the observations.

30 31 **i. Carbonate chemistry**

1 The uptake of ~26 % anthropogenic CO₂ by the global ocean (Friedlingstein et al., 2022) has
2 altered the oceanic carbonate chemistry over the past few decades (Iida et al., 2020).
3 Assessing how models correctly represent the oceanic carbonate chemistry is therefore critical
4 if we aim to derive accurate climate projections on their future change. The classical variables
5 for the study of carbonate chemistry are DIC, Alk, pH and pCO₂ (Williams and Follows,
6 2011). These variables are assessed in the mixed (DIC_{mixed}, Alk_{mixed}, pH_{mixed} and pCO_{2 mixed})
7 and mesopelagic (DIC_{meso}, Alk_{meso}, pH_{meso}) layers. The partial pressure of CO₂ is only
8 assessed in the mixed layer as the evaluation of pCO_{2 mixed} plays a critical role to assess the
9 skill of a BGC model to correctly represent the air-sea CO₂ flux.

11 **ii. Biological carbon pump**

13 The biological carbon pump is the transformation of nutrients and dissolved inorganic carbon
14 into organic carbon in the upper part of the ocean through phytoplankton photosynthesis and
15 the subsequent transfer of this organic material into the deep ocean. The functioning of this
16 pump relies on key pools of nutrients and carbon as well as several processes that control
17 mass fluxes between the pools. Changes in the biological carbon pump are now manifesting
18 globally (Capuzzo et al., 2018; Osman et al., 2019; Roxy et al., 2016).

20 An indirect evaluation of the model capability to capture key processes associated with the
21 biological carbon pump in the ocean upper layer, such as primary production, respiration, and
22 grazing consists in comparing the different ML pools [here the nutrients (NO_{3 mixed}, PO_{4 mixed},
23 Si_{mixed}), Chl_{mixed} and POC_{mixed}] with BGC-Argo observations. Similarly, the assessment of
24 the mesopelagic nutrients, and POC concentration (hereinafter denoted NO_{3 meso}, PO_{4 meso},
25 Si_{meso}, and POC_{meso}) provides an indirect evaluation of the key mesopelagic layer processes,
26 such as export production, respiration, etc.

28 In stratified systems, a DCM is formed at the base of the euphotic layer (Barbieux et al., 2019;
29 Cullen, 2015; Letelier et al., 2004; Mignot et al., 2014, 2011). It has been suggested that the
30 DCM plays a key role in the synthesis of organic carbon by phytoplankton (Macías et al.,
31 2014). DCMs are therefore key features to be assessed in BGC models with respect to
32 processes involved in the biological carbon pump such as the primary production. However
33 the DCM layer generally escapes detection by remote sensing. Furthermore, the DCM is also

1 an emergent feature that develops in response to complex physical and biogeochemical
2 interactions (Cullen, 2015). Thus, its evaluation provides critical information regarding the
3 accuracy of the model in capturing complex patterns of key ecosystem processes. The depth
4 and magnitude of DCM (H_{DCM} and Chl_{DCM}) are helpful metrics for the assessment of DCM
5 dynamics. The depth of the DCM is calculated as the depth where the maximum of Chl_a
6 occurs in the profile with the criterion that H_{DCM} should be deeper than the MLD. The
7 magnitude of the DCM is computed at the value at H_{DCM} .

8
9 NO_3 is often depleted in the surface layers and is a limiting factor for phytoplankton growth in
10 most oceanic regions. The vertical supply of NO_3 to the surface layers depends, among other
11 factors, on the vertical gradient of NO_3 (the nitracline), and, in particular, on its depth (the
12 nitracline depth) (Cermeno et al., 2008; Omand and Mahadevan, 2015). Therefore, the
13 comparison of the simulated nitracline depth (H_{nit}) with BGC-Argo observations allows for an
14 indirect assessment of the model performance in reproducing vertical fluxes of NO_3 .
15 Following previous studies (Cermeno et al., 2008; Lavigne et al., 2013; Richardson and
16 Bendtsen, 2019), the depth of the nitracline corresponds to the first depth where NO_3 is
17 detected. The detection threshold is set to $1 \mu\text{mol kg}^{-1}$, which corresponds to an upper
18 estimate of BGC-Argo NO_3 data accuracy (Johnson et al., 2017; Mignot et al., 2019).

19 20 **iii. Oxygen levels**

21
22 Oxygens levels in the global and coastal waters have declined over the whole water column
23 over the past decades (Schmidtko et al., 2017) and OMZs are expanding (Stramma et al.,
24 2008). Assessing how models correctly represent ocean oxygen levels as well as the OMZs is
25 therefore critical to monitor their change over time. Similarly to DCMs, the assessment of
26 OMZs is also informative on how the model simulates emergent dynamics as OMZs originate
27 from complex physical and biogeochemical interactions (Paulmier and Ruiz-Pino, 2009).
28 Oxygen levels are evaluated in the mixed ($O_{2 \text{ mixed}}$) and mesopelagic ($O_{2 \text{ meso}}$) layers. OMZs
29 are defined as oceanic regions where O_2 levels are lower than $20 \mu\text{mol kg}^{-1}$ (Paulmier and
30 Ruiz-Pino, 2009). OMZs are characterized by their depths ($H_{O_2\text{min}}$) and their concentrations
31 ($O_{2\text{min}}$).

32 33 **b. Bioregionalization of the model**

1
2 In this study, we use the K-means clustering algorithm (Hartigan and Wong, 1979) to
3 regionalize the ocean based on the modelled climatological monthly time series of the 23
4 metrics described previously. The K-means clustering is an unsupervised machine learning
5 algorithm that combine similar objects into a group in such a way that, within a group, the
6 similarity between objects is maximum and between groups, the similarity between objects is
7 minimum. This clustering tool has been successfully used to classify marine BGC regions in
8 different oceanic basins based on the seasonal cycle of satellite chlorophyll (Kheireddine et
9 al., 2021; Mayot et al., 2016; Lacour et al., 2015; D’Ortenzio and d’Alcala, 2009) . The step-
10 by-step methodology, used in this study, is described in the next section.

11
12 First, the climatological monthly time series of the 23 metrics were calculated at each model
13 grid cell from the climatological monthly time series of the state variables predicted by the
14 model from 2009 to 2017. The metrics in units of Chla or POC were log-10 transformed to
15 account for the fact that these metrics span several orders of magnitude and are lognormally
16 distributed. Second, to take into consideration the 6-month shift in seasons between the
17 northern and southern hemispheres, the dates for grid cells located in the Southern
18 Hemisphere were shifted by 6 months (Bock et al., 2022). Third, to classify the model grid
19 cells regardless of the different units of the 23 metrics, each metric was rescaled by
20 subtracting the global mean and by dividing the global standard deviation. As a result, each
21 metric had a mean of 0 and standard deviation of 1. Fourth, to reduce the dimensionality of
22 the data set, a principal component analysis was applied to the scaled data. Only the
23 components that explain 99 % of the variance in the data set were kept, reducing thereby the
24 dimensions of the data set by 85 %. A K-means clustering analysis was then performed on the
25 resulting data set. Following Kheireddine et al. (2021), the number of clusters was determined
26 based on a silhouette analysis (Rousseeuw, 1987), and, as a result, was set to 8 .

27

28 **c. Model efficiency**

29

30 To quantify the model predictive skill, a model efficiency statistical score (m_e) was computed
31 for each metric and in each BGC region:

32

$$m_e = 1 - \frac{\sum_{i=1}^N (m_i - o_i)^2}{\sum_{i=1}^N (o_i - \bar{o})^2}, \quad (3)$$

where m_i and o_i are the model and BGC-Argo matched values, respectively and \bar{o} is the BGC-Argo climatology. Assuming that the spatial variations are small in a given BGC-region, \bar{o} represents the temporal average and $\sum_{i=1}^N (o_i - \bar{o})^2$ represents the variance due to temporal fluctuations. The model efficiency tests whether the model outperforms the BGC-Argo climatology ($0 < m_e < 1$, Fennel et al., 2022), or stated differently, if the model-data mean square difference is lower than the observation variance, i.e., $\sum_{i=1}^N (m_i - o_i)^2 < \sum_{i=1}^N (o_i - \bar{o})^2$. To ensure the robustness of m_e , we verified that the number of matchups for each metric and in each BGC-region was greater than 100, then outliers were removed using Tukey's fences (Tukey, 1977).

4. Results and discussion

a. Global BGC-regions

The K-means clustering algorithm identified 8 distinct BGC-regions (Figure 2). 6 of the 8 BGC-regions correspond to well-defined spatial regions and are, thus, named accordingly, i.e., the Arctic, Equatorial, Mediterranean Sea, OMZs, Subtropical Gyres and Southern Oceans BGC-regions. The two others BGC-regions are located in the North Atlantic, North Pacific and North of the Southern Oceans BGC-region. These two BGC-regions correspond to ocean basins that are characterized by a phytoplankton "bloom" during spring time (Westberry et al., 2016), with the only difference that in one of the BGC-region, macronutrients such as nitrate and phosphate remains abundant throughout the year due to phytoplankton growth being mainly limited by iron (Williams and Follows, 2011). Accordingly, these two regions are named , Low Nutrients Bloom and High Nutrients Bloom, respectively. Finally, it should be noted that, outlier grid cells were no removed, and are mainly present in grid cells close to the coast. Furthermore, grid cells with bathymetry shallower than 1000 m, are not included in the clustering as metrics associated with the mesopelagic processes cannot be calculated in these shallow grid cells.

1 The BGC-regions found in study are overall coherent with the biomes estimated in Fay and
2 McKinley (2014) (hereinafter denoted FM2014). The Arctic and Southern Oceans correspond
3 to the FM2014 ice biome. The Subtropical Gyres correspond to the FM2014 subtropical
4 permanently stratified biome . The Equatorial BGC-region represents a larger area than the
5 Equatorial biome in FM2014. The Low Nutrients and High nutrients Bloom regions
6 correspond to FM2014 subtropical seasonally stratified and subpolar seasonally stratified
7 biomes, respectively. These two BGC-regions are coherent in the North Pacific and in the
8 Southern Ocean in both studies. They differ, however, in the North Atlantic. In FM2014, the
9 subpolar North Atlantic is divided between the subtropical seasonally stratified and subpolar
10 seasonally stratified biomes, whereas in our study this area is only represented by one BGC-
11 region; the Low Nutrients Bloom region. Finally, the Mediterranean sea and OMZs BGC-
12 regions are not represented in FM2014. The main differences observed between our study
13 and FM2014 stem from the fact our bioregionalization is based on 23 input variables while
14 the clustering in FM14 is only based on one BGC input variable (Chla) and three physical
15 variables (sea surface temperature, MLD and sea-ice fraction). Therefore, our methodology
16 can identified specific BGC-regions whose function is mainly characterized by variables other
17 than Chla (e.g. OMZs). Our method also include coastal areas, and identify the
18 Mediterranean Sea which is not included in FM2014 because it is considered as a coastal
19 region.

20

21 **b. Model performance**

22

23 Figures 3-5 show the m_e calculated for each assessment metric and in each BGC region. For
24 clarity, the m_e are grouped by process (carbonate chemistry, biological carbon pump and
25 oxygen levels). The results are presented as bubble plots (panels b) where the size of the
26 bubble is proportional to the value of m_e . For a given assessment metric, the median value of
27 m_e over all BGC regions are represented as a bar plot (panels c). Similarly, for a given BGC
28 region, the median value of m_e over all assessment metrics is represented as a bar plot (panels
29 a). When the number of assessment metrics is lower than 3, the mean value is computed
30 instead of the median. In panels b, The x and y axes are arranged in descending order of the
31 median value of m_e over all assessment metrics (panels a) and the median value of m_e over
32 all BGC regions (panel b), respectively.

33

i. Carbonate chemistry

Overall, the model results in better predictions for Alk_{meso} , $\text{DIC}_{\text{mixed}}$, $\text{Alk}_{\text{mixed}}$, DIC_{meso} and pH_{meso} than the BGC-Argo climatology ($m_e > 1$) (Figs. 3b and 3C). The median m_e value for these metrics are (0.84, 0.78, 0.60, 0.57, and 0.56). For pH_{meso} , the model outperforms the BGC-Argo climatology in all BGC-regions. For Alk_{meso} , $\text{DIC}_{\text{mixed}}$, $\text{Alk}_{\text{mixed}}$, the model errors are lower than the variability of the observations everywhere except in the Arctic BGC-region. DIC_{meso} is better predicted by the model than the BGC-Argo climatology in almost all BGC-regions except in the Arctic, Southern Oceans, and the Mediterranean Sea. The model's ability to reproduce the instantaneous variability of pH_{mixed} and $\text{pCO}_2_{\text{mixed}}$ is more limited. The model outperform the BGC-Argo climatology in only 4 BGC-regions for pH_{mixed} and 2 BGC-regions for $\text{pCO}_2_{\text{mixed}}$. Overall, the carbonate chemistry dynamics is better estimated by the model than the BGC-Argo climatology in all BGC-regions except in the Arctic BGC-region (Fig. 3a)

ii. Biological carbon pump

The model efficiency is more limited for the biological carbon pump (Figs 4b and 4c). The model results in significant better estimations than the BGC-Argo climatology only for nutrients in the mesopelagic layer (Si_{meso} , $\text{PO}_4_{\text{meso}}$ and $\text{NO}_3_{\text{meso}}$), and H_{nit} (Fig. 4c). The model efficiency in predicting nutrients deteriorates when we move from the mesopelagic to the mixed layer, where the median m_e values drop from 0.83, 0.78, 0.68 to -2.10 and 0.1, 0.08 for Si, PO_4 and NO_3 respectively. For the metrics associated with the first trophic level (i.e., $\text{Chl}_{\text{mixed}}$, H_{DCM} , Chl_{DCM} , $\text{POC}_{\text{mixed}}$, and POC_{meso}), the median m_e values are lower than 0 in almost all BGC-regions, suggesting than the model is almost systematically outperformed by the BGC-Argo climatology. Regionally, the median m_e values are greater than 1 only in the Low Nutrients and High Nutrients Bloom, the Mediterranean Sea and the OMZs BGC-regions.

iii. Oxygen levels

The model errors for $\text{O}_2_{\text{mixed}}$ are lower than the data variability in all BGC-regions (Fig. 5b). In the mesopelagic layer, the model results also in better predictions than the BGC-Argo

1 climatology everywhere except in the Southern Oceans and in the Arctic BGC-regions. The
2 Oxygen Minimum Zones are detected in both the Equatorial and OMZs BGC regions. The
3 magnitude of OMZs in both regions are better represented by the BGC-Argo climatology than
4 the model, whereas the depth of the OMZ is better predicted by the model only in the OMZs
5 region.

7 **iv. Discussion**

8
9 The skill of the model to surpass the BGC-Argo climatology for DIC, Alk and O₂ in the
10 mesopelagic and the mixed layers is not surprising. As detailed in the appendix, the model
11 applies a climatological damping,- to NO₃, PO₄, O₂, Si - with World Ocean Atlas 2013
12 (Garcia et al., 2013, 2014) - and to DIC and Alk- with GLODAPv2 climatology (Key et al.,
13 2015). The damping mitigates the impact of the physical data assimilation in the offline
14 coupled hydrodynamic-biogeochemical system, that results in an unrealistic drift of various
15 biogeochemical variables (Fennel et al., 2019; Park et al., 2018; Gasparin et al., 2021).

16
17 Following this reasoning, one should also expect the nutrients to be better estimated by the
18 model than by the BGC-Argo climatology. While, this is true in the mesopelagic layer, the
19 model performance is significantly deteriorated in the mixed layer. In addition to the
20 climatological damping, the model also embeds a reduced order Kalman filter (Lellouche et
21 al., 2013) that assimilates daily L4 remotely sensed surface Chl_a that provide a correction in
22 the mixed layer to the modelled Chl_a (both in the nanophytoplankton and diatom
23 compartments) as well as to nitrate through the use of model error covariance. We verified
24 that the assimilation of satellite Chl_a decrease the model-BGC-argo data misfit comparing to
25 a simulation without assimilation (not shown). We can, therefore speculate that uncertain
26 model error covariance during the assimilation of satellite Chl_a degrades the model skill in
27 predicting ML nutrients. This hypothesis could be tested by computing the model efficiencies
28 for a model simulation with only the climatological damping activated.

29
30 While the assimilation decreases the model-BGC-argo data misfit for Chl_{mixed} comparing to a
31 simulation without assimilation (not shown), the model errors for the three metrics associated
32 with Chl_a remains systematically larger than the BGC-Argo variability. Yet, it has been
33 shown that, when comparing to the satellite Chl_a product assimilated (European Union-

1 Copernicus Marine Service, 2022), the model-satellite misfit was lower than the variability of
2 the satellite data (European Union-Copernicus Marine Service, 2019). This suggest that the
3 model-BGC-Argo data misfit could originate, in part, from discrepancies between the satellite
4 Chla product assimilated and the BGC-Argo data. We propose that studies should check the
5 consistency between ocean colour products and BGC-Argo Chla products at the global scale
6 as these two products are expected to be assimilated together in future operational BGC
7 systems (Ford, 2021).

8
9 Overall, the model also performs worse than the BGC-Argo climatology in predicting POC
10 concentrations, the OMZs, pH_{mixed} and $\text{pCO}_2_{\text{mixed}}$. The poor performance of PISCES-based
11 models relative to BGC-Argo POC observations has been extensively studied in Gali et al.
12 (2022). They pointed out that the large model-data misfit could be the result of an imperfect
13 BGC-Argo POC- bp conversion factor, unsuitable model parameters associated with POC
14 dynamics and missing processes in the model structure. Similarly, the poor model skill in
15 capturing the OMZs dynamics are also already been documented in several studies (Busecke
16 et al., 2022; Schmidt et al., 2021; Cabré et al., 2015). All studies suggested that improving the
17 ocean circulation in physical models may be the most important factor to improve the
18 accuracy of OMZs model predictions. Finally, the negative model efficiencies for pH_{mixed} and
19 $\text{pCO}_2_{\text{mixed}}$ could be understood by considering that pH and pCO_2 are driven by DIC, Alk,
20 temperature and salinity. Consequently, the model uncertainties in pH_{mixed} and $\text{pCO}_2_{\text{mixed}}$ are
21 also controlled by the model errors in these 4 variables. Therefore, even small errors in
22 modelled DIC, Alk (Fig. 3b) as well as modelled temperature and salinity (Lellouche et al.,
23 2018) could lead to a poor model performance in capturing the variability of pH and pCO_2 .

24 25 26 **c. Recommendation for the design of the BGC-Argo** 27 **observing system**

28
29 Observing System Simulation Experiments (OSSE) have been the primary tool to inform
30 about the design of the BGC-Argo observing system (Ford, 2021; Biogeochemical-Argo
31 Planning Group, 2016). OSSEs typically comprises a realistic “nature run”, which represents
32 “the truth” from which synthetic observations are sampled. The synthetic observations
33 represents the observing system to be designed. To test its impact on improving models

1 predictive skill, the synthetic observations are then assimilated in an “assimilative run”. The
2 accuracy of the “assimilative run” is then evaluated against the “nature run”. Here, we use the
3 real BGC-Argo observations to inform about the design of the BGC-Argo network. More
4 specifically, our aim is to inform about the regions where the model errors are greater than the
5 variability of the BGC-Argo data, and consequently where BGC-Argo observations should be
6 enhanced to improve the model accuracy through BGC-Argo data assimilation or process-
7 oriented assessment studies.

8
9 For a given BGC-region, we compute a single multivariate score which correspond to the
10 median of the 23 m_e associated with each assessment metric (Fig. 6). This is consistent with
11 the fact that the BGC-Argo floats, that are now deployed, observe the 5 variables used to
12 derive the assessments metrics, i.e., O_2 , $Chla$, NO_3 , b_{bp} and pH . The Arctic BGC-region is the
13 only region whose median m_e is negative (-0.75). This is consistent with the fact that only 4
14 assessment metrics (namely NO_3 meso, POC meso, pH meso, pH mixed) are better represented by the
15 model than the BGC-Argo climatology in this region (Figs. 3 and 4). Few BGC-Argo
16 observations exist in this region (Fig.1), and, the winter-spring months are particularly under-
17 sampled (not shown). In this region, satellite observations of $Chla$ are not possible most of
18 year and the scarcity of in situ observations probably make the climatological damping less
19 efficient in this region. Given the rapid changes occurring in the Arctic biogeochemical
20 processes and ecosystems due to climate change (Solan et al., 2020), we strongly recommend
21 to enhance the Arctic region with BGC-Argo floats. These observations are critical to better
22 constrain the model. Given also the key role of the Southern Oceans and the Equatorial
23 regions for the oceanic CO_2 cycle (Long et al., 2021; Landschützer et al., 2014), we also
24 recommend to enhance these two regions whose median m_e are barely greater than 0 (0.04
25 and 0.12, respectively).

26 27 **5. Conclusion**

28
29 In this study, we propose a method based on the global data set of BGC-Argo observations, a
30 K-means clustering algorithm and 23 assessments metrics to simplify model-data comparison
31 and inform on Copernicus Marine Service forecasting system predictive skill and the design
32 of the BGC-Argo observing system. The K-means algorithm identified 8 BGC-regions in the
33 model simulation that are consistent with Fay and McKinley (2014) study. Within each

1 BGC-region and for each assessment metric, we compute a model efficiency statistical score
2 that quantify whether the model outperforms the BGC-Argo climatology by comparing the
3 model-BGC-Argo data mean square difference with the observation variance.

4
5 Overall, the model surpasses the BGC-Argo climatology in predicting pH, DIC, Alk and O₂ in
6 the mesopelagic and the mixed layers, as well as NO₃, Si and PO₄ in the mesopelagic layer.
7 Concerning the other metrics, whose model predictions are outperformed by the BGC-Argo
8 climatology, we provide suggestions to reduce the model-data misfit and thus to increase the
9 model efficiency. For, PO₄, Si, and NO₃, we propose to test if the uncertain model error
10 covariances during the assimilation of satellite Chl_a could lead to a degradation in predicting
11 nutrients in the mixed layer. For Chl_a-related metrics, we recommend to check the
12 consistency between ocean colour products and BGC-Argo Chl_a products at the global scale
13 as it may explain part of the misfit between the model, that assimilates satellite Chl_a, and
14 BGC-Argo observations. The discrepancies between modelled and observed POC and OMZs
15 have been already investigated in previous studies. It has been suggested that improving the
16 BGC-Argo POC-b_{bp} conversion factor, tuning the model parameters and implementing
17 missing processes in the model structure could decrease the model-data inconsistencies
18 associated with POC dynamics. Similarly, the improvement of the ocean circulation in
19 physical models should improve the accuracy of OMZs model predictions. Finally, pH_{mixed}
20 and pCO_{2 mixed} should be better modelled if the uncertainties associated with DIC, Alk,
21 temperature and salinity in the mixed layer are reduced.

22
23 The method proposed here is also beneficial to inform about the BGC-Argo network design.
24 In particular, the regions where BGC-Argo observations should be enhanced to reduce the
25 model-data misfit through the assimilation of BGC-Argo data or process-oriented assessment
26 studies. We strongly recommend to enhance the Arctic region, which is critically under
27 sampled and is constantly outperformed by the BGC-Argo climatology. Likewise, BGC-Argo
28 observations should be enriched in the Equatorial region and in the Southern Oceans, two
29 regions where the model error barely exceed the BGC-Argo observations variability.

1 **Tables**

2

3 **Table 1.** Data mode and QC flags of the BGC-Argo observations used in this study. In the
 4 Argo data-system, the data are available in three data modes, “Real-Time”, ”Adjusted” and
 5 ”Delayed”. See section 2a for a brief description of each data mode. The flags “3” and “4”
 6 refers to “potentially bad data “ and “bad data”, respectively. See also Bittig et al. (2019), for
 7 a more detailed description of Argo data modes and flags.

8

Parameter	Data mode	Data mode of associated pressure, temperature and salinity profiles	QC flags
Chl <i>a</i>	Adjusted and Delayed	Real time, Adjusted and Delayed	<ul style="list-style-type: none"> • Real time: All flags except 4 • Adjusted or Delayed: All flags except 3 and 4
O ₂	Delayed	Delayed	<ul style="list-style-type: none"> • All flags except 3 and 4
NO ₃	Adjusted and Delayed	Real time, Adjusted and Delayed	<ul style="list-style-type: none"> • Real time: All flags except 4 • Adjusted or Delayed: All flags except 3 and 4
pH	Adjusted and Delayed	Real time, Adjusted and Delayed	<ul style="list-style-type: none"> • Real time: All flags except 4 • Adjusted or Delayed: All flags except 3 and 4
b _{bp}	Real time and Delayed	Real time, Adjusted and Delayed	<ul style="list-style-type: none"> • Real time: All flags except 4 • Adjusted or Delayed (P,T,S): All flags except 3 and 4

- Adjusted or Delayed (b_{bp}):
All flags 4
-

1

1
2
3
4

Table 2. Assessment metrics used to assess the model simulation with BGC-Argo data . For each metric, the level of assessment, as described in Hipsey et al. (2020) is also indicated.

Process	Metric	Definition	units	Assessment level
Carbonate chemistry	pCO _{2 mixed}	Depth-averaged pCO ₂ in the mixed layer	µatm	State variable
	DIC _{mixed}	Depth-averaged DIC in the mixed layer	µmol kg ⁻¹	State variable
	Alk _{mixed}	Depth-averaged Alk in the mixed layer	µmol kg ⁻¹	State variable
	DIC _{meso}	Depth-averaged DIC in the mesopelagic layer	µmol kg ⁻¹	State variable
	Alk _{meso}	Depth-averaged Alk in the mesopelagic layer	µmol kg ⁻¹	State variable
	pH _{mixed}	Depth-averaged pH in the mixed layer	total	State variable
	pH _{meso}	Depth-averaged pH in the mesopelagic layer	total	State variable
Biological carbon pump	Chl _{mixed}	Depth-averaged Chl _a in the mixed layer	mg m ⁻³	State variable
	NO _{3 mixed}	Depth-averaged NO ₃ in the mixed layer	µmol kg ⁻¹	State variable
	PO _{4 mixed}	Depth-averaged PO ₄ in the mixed layer	µmol kg ⁻¹	State variable
	Si _{mixed}	Depth-averaged Si in the mixed layer	µmol kg ⁻¹	State variable

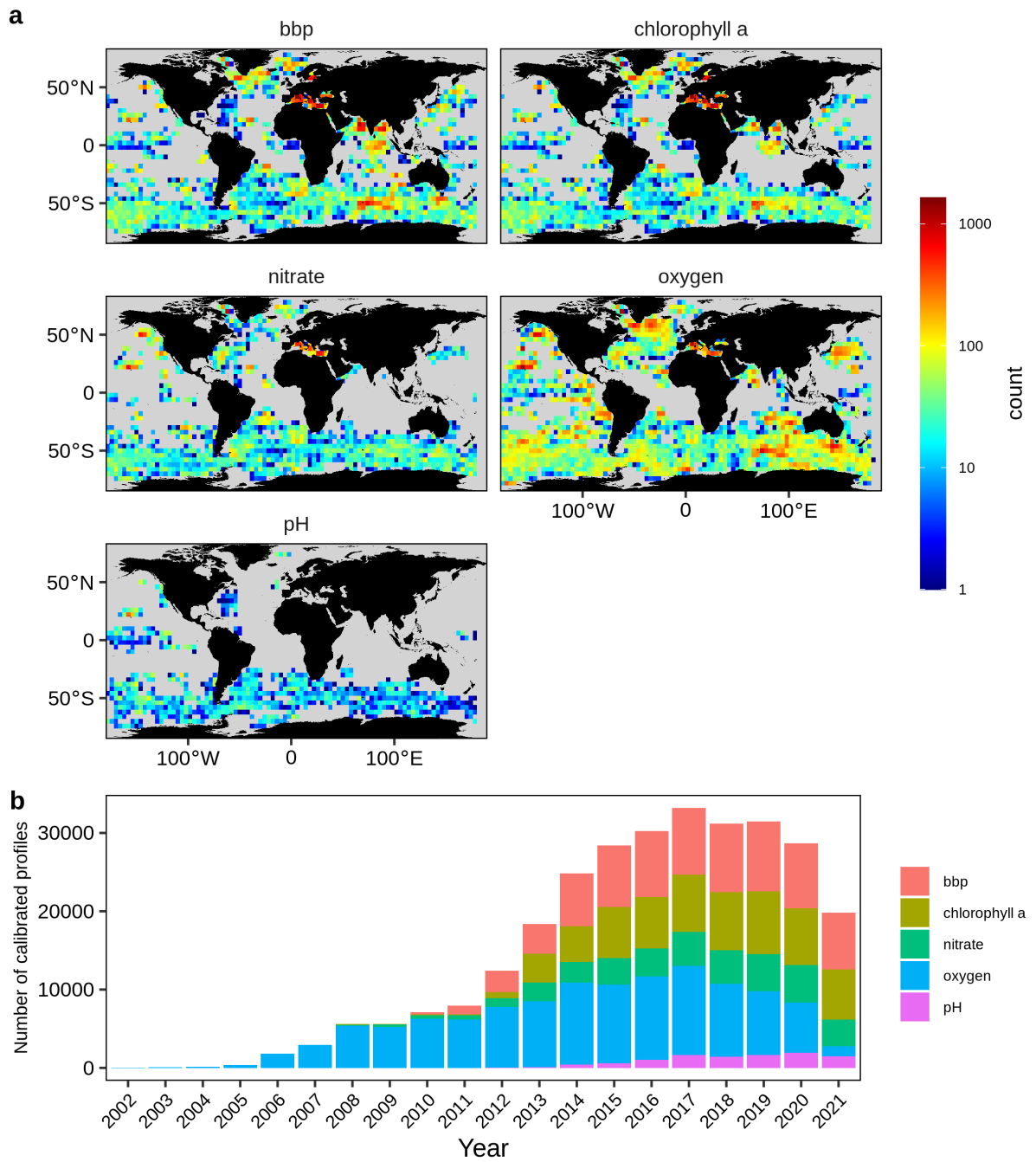
	$\text{NO}_3_{\text{meso}}$	Depth-averaged NO_3 in the mesopelagic layer	$\mu\text{mol kg}^{-1}$	State variable
	$\text{PO}_4_{\text{meso}}$	Depth-averaged PO_4 in the mesopelagic layer	$\mu\text{mol kg}^{-1}$	State variable
	Si_{meso}	Depth-averaged Si in the mesopelagic layer	$\mu\text{mol kg}^{-1}$	State variable
	$\text{POC}_{\text{mixed}}$	Depth-averaged POC in the mixed layer	mg m^{-3}	State variable
	POC_{meso}	Depth-averaged POC in the mesopelagic layer	mg m^{-3}	State variable
	Chl_{DCM}	Magnitude of DCM	mg m^{-3}	Emergent property
	H_{DCM}	Depth of DCM	m	Emergent property
	H_{nit}	Depth of nitracline	m	Emergent property
Oxygen levels	$\text{O}_2_{\text{mixed}}$	Depth-averaged O_2 in the mixed layer	$\mu\text{mol kg}^{-1}$	State variable
	O_2_{meso}	Depth-averaged O_2 in the mesopelagic layer	$\mu\text{mol kg}^{-1}$	State variable
	$\text{O}_{2\text{min}}$	value of O_2 minimum	$\mu\text{mol kg}^{-1}$	Emergent property
	$\text{H}_{\text{O}_2\text{min}}$	Depth of O_2 minimum	m	Emergent property

1

2

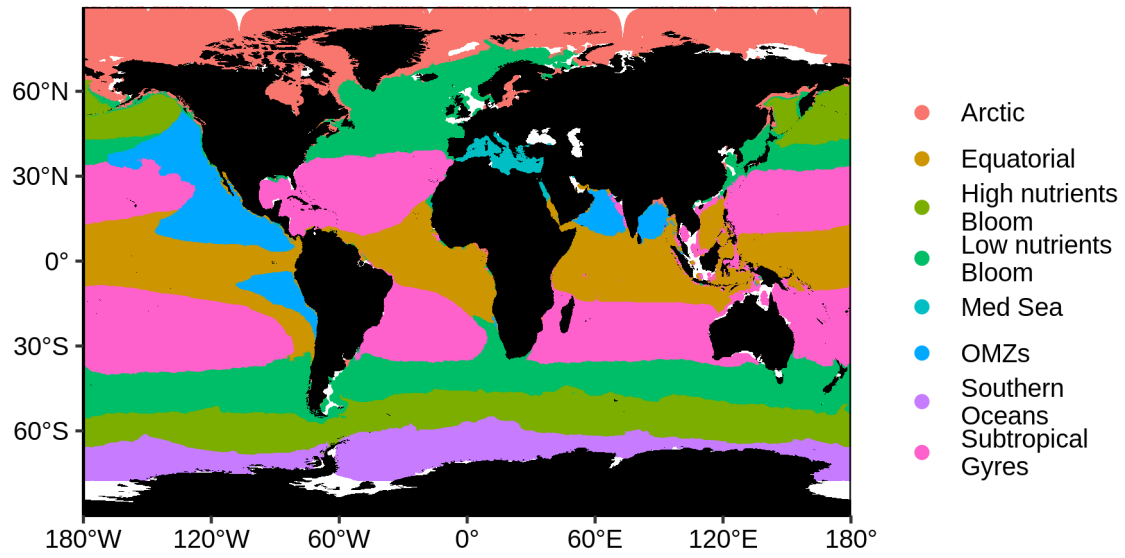
1 Figures

2



3

4 **Figure 1.** Spatial and temporal coverage of quality-controlled BGC-Argo pH, NO₃⁻, Chla, O₂,
5 and b_{bp} profiles. **(a)** Number of quality-controlled profiles for the entire period per 4°x4° bin.
6 **(b)** Number of quality-controlled profiles per year.

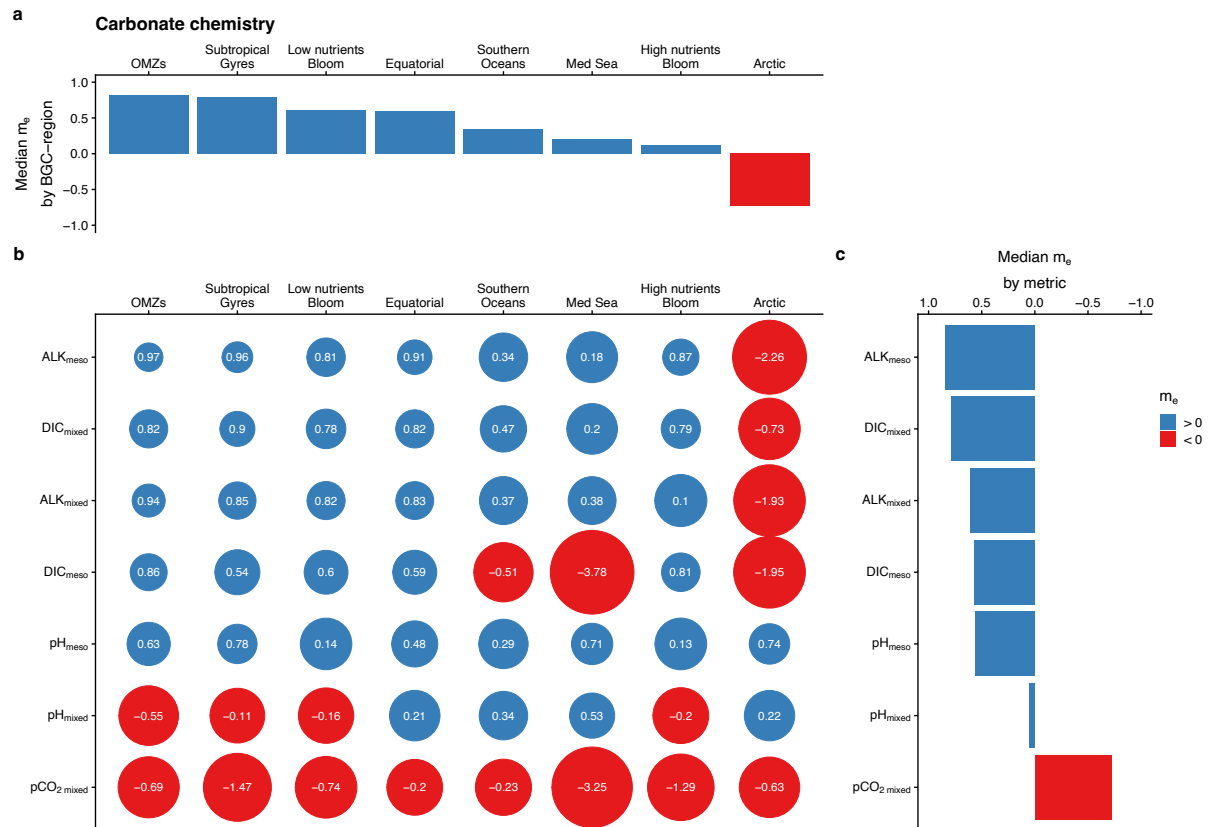


1

2 **Figure 2.** Spatial distribution of the 8 BGC-regions obtained with a K-means clustering
 3 method applied to a dataset of modelled climatological monthly time series of the 23
 4 assessment metrics.

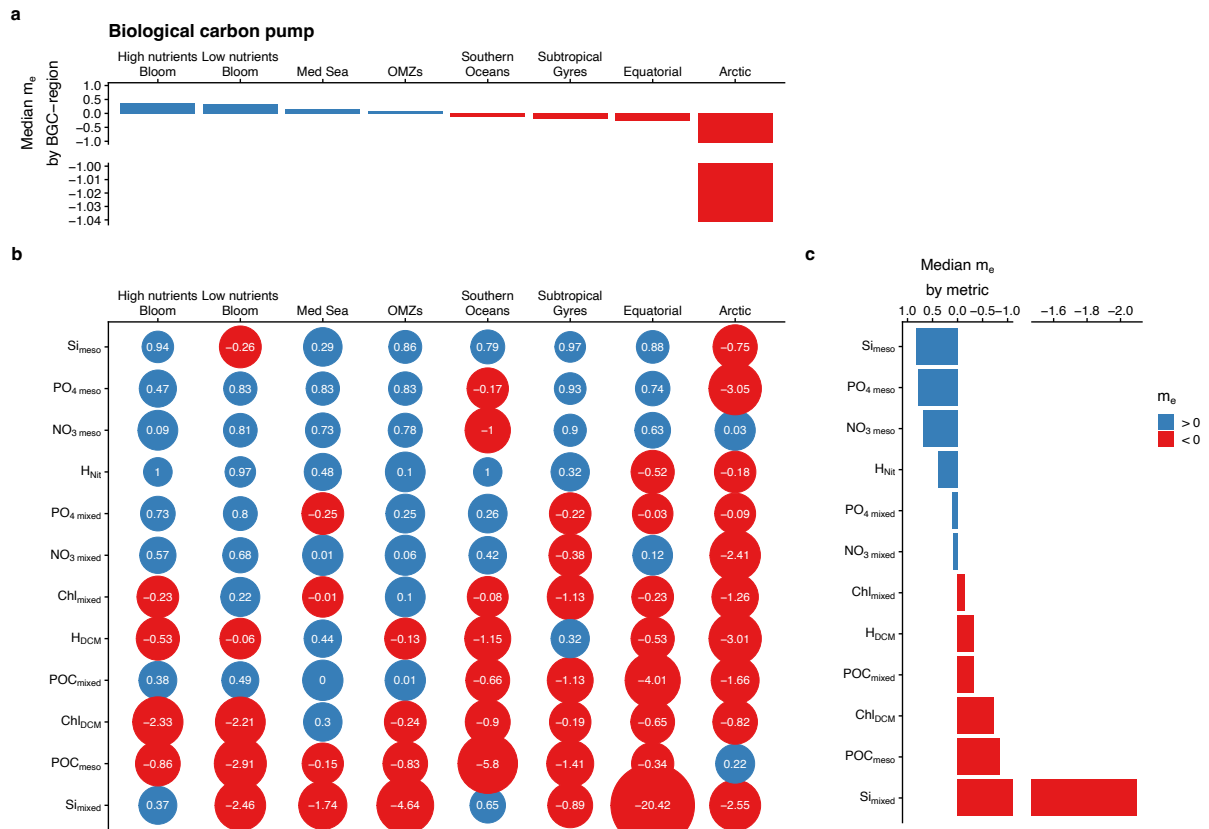
5

6

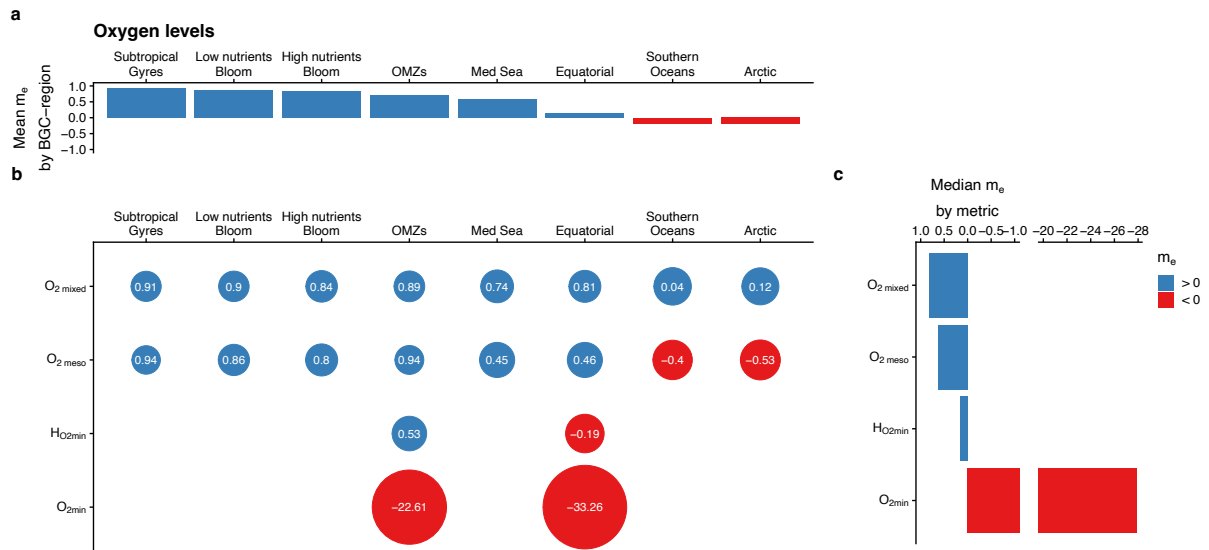


1
 2 **Figure 3.** Bubble plot of model efficiency statistical score (m_e) as a function of BGC-regions
 3 and assessment metrics associated with the carbonate chemistry (**b**). The size of a bubble is
 4 proportional to the value of m_e . For a given assessment metric, the median value of m_e over
 5 all BGC regions are represented as a bar plot (**c**). Similarly, for a given BGC region, the
 6 median value of m_e over all assessment metrics is represented as a bar plot (**a**). In (**b**), The x
 7 and y axes are arranged in descending order of the median value of m_e over all assessment
 8 metrics (panels a) and the median value of m_e over all BGC regions, respectively. The blue
 9 and red colours correspond to a positive and negative m_e .

10

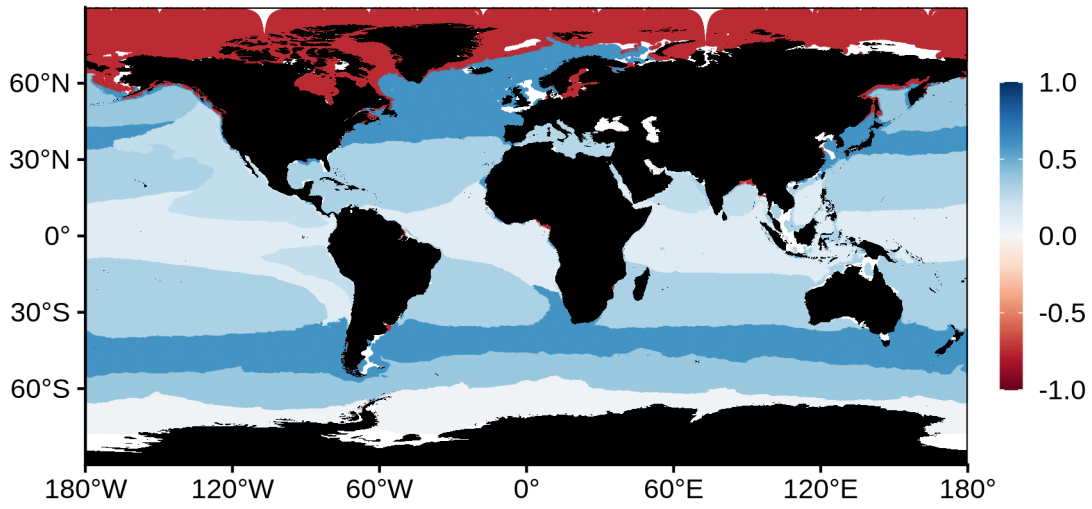


1
2 **Figure 4.** Same as Figure 3 but for assessment metrics associated with the biological carbon
3 pump.
4



1
 2 **Figure 5.** Same as Figure 3 but for assessment metrics associated with the oxygen levels.
 3 Note that in (a), the bar plot represents the mean value of m_e over all assessment metrics.
 4

Median model efficiency



1

2 **Figure 6.** Median of the 23 m_e associated with each assessment metric by BGC-region.

1 **Appendix**

2

3 **A.1 The CMEMS global hydrodynamic-biogeochemical model**

4

5 The model used in this study features the offline coupled NEMO–PISCES model, with a $1/4^\circ$
6 horizontal resolution 50 vertical levels (with 22 levels in the upper 100 m, the vertical
7 resolution is 1m near the surface and decreases to 450m resolution near the bottom) and daily
8 temporal resolution, covering the period from 2009 to 2017.

9

10 The biogeochemical model PISCES v2 (Aumont et al., 2015) is a model of intermediate
11 complexity designed for global ocean applications, and is part of NEMO modelling platform.
12 It features 24 prognostic variables and includes five nutrients that limit phytoplankton growth
13 (nitrate, ammonium, phosphate, silicate and iron) and four living compartments: two
14 phytoplankton size classes (nanophytoplankton and diatoms, resp. small and large) and two
15 zooplankton size classes (microzooplankton and mesozooplankton, resp. small and large); the
16 bacterial pool is not explicitly modelled. PISCES distinguishes three non-living detrital pools
17 for organic carbon, particles of calcium carbonate and biogenic silicate. Additionally, the
18 model simulates the carbonate system and dissolved oxygen. PISCES has been successfully
19 used in a variety of biogeochemical studies, both at regional and global scale (Bopp et al.,
20 2005; Gehlen et al., 2006, 2007; Gutknecht et al., 2019; Lefèvre et al., 2019; Schneider et al.,
21 2008; Séférian et al., 2013; Steinacher et al., 2010; Tagliabue et al., 2010).

22

23 The dynamical component is the latest Mercator Ocean global $1/12^\circ$ high-resolution ocean
24 model system, extensively described and validated in Lellouche et al. (2013, 2018). This
25 system provides daily and $1/4^\circ$ -coarsened fields of horizontal and vertical current velocities,
26 vertical eddy diffusivity, mixed layer depth, sea ice fraction, potential temperature, salinity,
27 sea surface height, surface wind speed, freshwater fluxes and net surface solar shortwave
28 irradiance that drive the transport of biogeochemical tracers. This system also features a
29 reduced-order Kalman filter based on the Singular Evolutive Extended Kalman filter (SEEK)
30 formulation introduced by Pham et al. (1998), that assimilates, on a 7-day assimilation cycle,
31 along-track altimeter data, satellite Sea Surface Temperature and Sea-Ice Concentration from

1 OSTIA, and *in situ* temperature and salinity vertical profiles from the CORA 4.2 *in situ*
2 database.

3

4 In addition, the biogeochemical component of the coupled system also embeds a reduced
5 order Kalman filter (similar to the above mentioned) that operationally assimilates daily L4
6 remotely sensed surface chlorophyll (European Union-Copernicus Marine Service, 2022).
7 Thanks to a multivariate formulation of model error covariances, the system is able to provide
8 a 3D correction to the nanophytoplankton, diatoms and nitrates model concentrations, from
9 the surface chlorophyll data provided by satellite observations.

10 In parallel, a climatological-damping is applied to nitrate, phosphate, oxygen, silicate - with
11 World Ocean Atlas 2013 - to dissolved inorganic carbon and alkalinity – with GLODAPv2
12 climatology (Key et al., 2015) - and to dissolved organic carbon and iron - with a 4000-year
13 PISCES climatological run. This relaxation is set to mitigate the impact of the physical data
14 assimilation in the offline coupled hydrodynamic-biogeochemical system, leading significant
15 rises of nutrients in the Equatorial Belt area, and resulting in an unrealistic drift of various
16 biogeochemical variables e.g. chlorophyll, nitrate, phosphate (Fennel et al., 2019; Park et al.,
17 2018). The time-scale associated with this climatological damping is set to 1 year and allows
18 a smooth constraint that has been shown to be efficient to reduce the model drift.

19

1 **Data availability.** The BGC model data can be downloaded from the Copernicus Marine
2 Environmental Monitoring Service
3 (https://resources.marine.copernicus.eu/?option=com_csw&view=details&product_id=GLOB
4 [AL_ANALYSIS_FORECAST_BIO_001_028](https://resources.marine.copernicus.eu/?option=com_csw&view=details&product_id=GLOB)). The BGC-Argo data were downloaded from
5 the Argo Global Data Assembly Centre in France (<ftp://ftp.ifremer.fr/argo/>).
6

7 **Authors Contribution:** AM, GC, FD, SS and VT originated the study. AM, HC, FD, RS and
8 VT designated the study. AM and RS process the BGC-Argo floats data. AM analysed the
9 data. AM wrote the first draft of the manuscript. HC, GC, FD, EG, PL, CP, SS,RS,VT and AT
10 contributed to the subsequent drafts. All authors read and approved the final draft.
11

12 **Competing Interests:** The authors declare no competing financial interests.
13

14 **Materials and correspondence:** Correspondence and request for material should be
15 addressed to mignot@mercator-ocean.fr
16

17 **Acknowledgements:** This study has been conducted using the Copernicus Marine Service
18 products. The BGC-Argo data were collected and made freely available by the International
19 Argo program and the national programs that contribute to it (<https://www.argo.jcommops.org>). The Argo program is part of the Global Ocean Observing System. Part of this work was
20 performed within the framework of the BIOOPTIMOD and MASSIMILI CMEMS Service
21 Evolution Projects. This paper represents a contribution to the following research projects:
22 NAOS (funded by the Agence Nationale de la Recherche in the framework of the French
23 “Equipement d’avenir” program, grant ANR J11R107-F), remOcean (funded by the European
24 Research Council, grant 246777), and the French Bio-Argo program (BGC-Argo France;
25 funded by CNES-TOSCA, LEFE-GMMC).
26
27
28

1 **References**

2

3 Allen, J. I., Somerfield, P. J., and Gilbert, F. J.: Quantifying uncertainty in high-resolution
4 coupled hydrodynamic-ecosystem models, *J. Mar. Syst.*, 64, 3–14,
5 <https://doi.org/10.1016/j.jmarsys.2006.02.010>, 2007.

6 Aumont, O., Ethé, C., Tagliabue, A., Bopp, L., and Gehlen, M.: PISCES-v2: an ocean
7 biogeochemical model for carbon and ecosystem studies, *Geosci. Model Dev.*, 8, 2465–2513,
8 <https://doi.org/10.5194/gmd-8-2465-2015>, 2015.

9 Barbieux, M., Uitz, J., Gentili, B., Pasqueron de Fommervault, O., Mignot, A., Poteau, A.,
10 Schmechtig, C., Taillandier, V., Leymarie, E., Penker'h, C.,
11 D'Ortenzio, F., Claustre, H., and Bricaud, A.: Bio-optical characterization of
12 subsurface chlorophyll maxima in the Mediterranean Sea from a Biogeochemical-Argo float
13 database, *Biogeosciences*, 16, 1321–1342, <https://doi.org/10.5194/bg-16-1321-2019>, 2019.

14 Biogeochemical-Argo Planning Group: The scientific rationale, design and implementation
15 plan for a Biogeochemical-Argo float array, <https://doi.org/10.13155/46601>, 2016.

16 Bittig, H. C., Steinhoff, T., Claustre, H., Fiedler, B., Williams, N. L., Sauzède, R., Körtzinger,
17 A., and Gattuso, J.-P.: An alternative to static climatologies: robust estimation of open ocean
18 CO₂ variables and nutrient concentrations from T, S, and O₂ data using Bayesian neural
19 networks, *Front. Mar. Sci.*, 5, 328, 2018.

20 Bittig, H. C., Maurer, T. L., Plant, J. N., Wong, A. P., Schmechtig, C., Claustre, H., Trull, T.
21 W., Udaya Bhaskar, T. V. S., Boss, E., and Dall’Olmo, G.: A BGC-Argo guide: Planning,
22 deployment, data handling and usage, *Front. Mar. Sci.*, 6, 502, 2019.

23 Bock, N., Cornec, M., Claustre, H., and Duhamel, S.: Biogeographical Classification of the
24 Global Ocean From BGC-Argo Floats, *Glob. Biogeochem. Cycles*, 36,
25 <https://doi.org/10.1029/2021GB007233>, 2022.

26 Bojinski, S., Verstraete, M., Peterson, T. C., Richter, C., Simmons, A., and Zemp, M.: The
27 concept of essential climate variables in support of climate research, applications, and policy,
28 *Bull. Am. Meteorol. Soc.*, 95, 1431–1443, 2014.

29 Bopp, L., Aumont, O., Cadule, P., Alvain, S., and Gehlen, M.: Response of diatoms
30 distribution to global warming and potential implications: A global model study, *Geophys.*
31 *Res. Lett.*, 32, <https://doi.org/10.1029/2005GL023653>, 2005.

32 Boyer, T. P., Antonov, J. I., Baranova, O. K., Garcia, H. E., Johnson, D. R., Mishonov, A. V.,
33 O’Brien, T. D., Seidov, D., Smolyar, I., and Zweng, M. M.: World ocean database 2013,
34 2013.

35 Breitburg, D., Levin, L. A., Oschlies, A., Grégoire, M., Chavez, F. P., Conley, D. J., Garçon,
36 V., Gilbert, D., Gutiérrez, D., Isensee, K., Jacinto, G. S., Limburg, K. E., Montes, I., Naqvi, S.
37 W. A., Pitcher, G. C., Rabalais, N. N., Roman, M. R., Rose, K. A., Seibel, B. A., Telszewski,
38 M., Yasuhara, M., and Zhang, J.: Declining oxygen in the global ocean and coastal waters,
39 *Science*, 359, <https://doi.org/10.1126/science.aam7240>, 2018.

- 1 Briggs, N., Perry, M. J., Cetinić, I., Lee, C., D'Asaro, E., Gray, A. M., and Rehm, E.: High-
2 resolution observations of aggregate flux during a sub-polar North Atlantic spring bloom,
3 *Deep Sea Res. Part Oceanogr. Res. Pap.*, 58, 1031–1039,
4 <https://doi.org/10.1016/j.dsr.2011.07.007>, 2011.
- 5 Busecke, J. J. M., Resplandy, L., Ditkovsky, S. J., and John, J. G.: Diverging Fates of the
6 Pacific Ocean Oxygen Minimum Zone and Its Core in a Warming World, *AGU Adv.*, 3,
7 <https://doi.org/10.1029/2021AV000470>, 2022.
- 8 Cabré, A., Marinov, I., Bernardello, R., and Bianchi, D.: Oxygen minimum zones in the
9 tropical Pacific across CMIP5 models: mean state differences and climate change trends,
10 *Biogeosciences*, 12, 5429–5454, <https://doi.org/10.5194/bg-12-5429-2015>, 2015.
- 11 Capuzzo, E., Lynam, C. P., Barry, J., Stephens, D., Forster, R. M., Greenwood, N.,
12 McQuatters-Gollop, A., Silva, T., van Leeuwen, S. M., and Engelhard, G. H.: A decline in
13 primary production in the North Sea over 25 years, associated with reductions in zooplankton
14 abundance and fish stock recruitment, *Glob. Change Biol.*, 24, e352–e364,
15 <https://doi.org/10.1111/gcb.13916>, 2018.
- 16 Cermeno, P., Dutkiewicz, S., Harris, R. P., Follows, M., Schofield, O., and Falkowski, P. G.:
17 The role of nutricline depth in regulating the ocean carbon cycle, *Proc. Natl. Acad. Sci.*, 105,
18 20344–20349, <https://doi.org/10.1073/pnas.0811302106>, 2008.
- 19 Claustre, H., Johnson, K. S., and Takeshita, Y.: Observing the Global Ocean with
20 Biogeochemical-Argo, *Annu. Rev. Mar. Sci.*, 12, annurev-marine-010419-010956,
21 <https://doi.org/10.1146/annurev-marine-010419-010956>, 2020.
- 22 Crowder, L. B., Hazen, E. L., Avissar, N., Bjorkland, R., Latanich, C., and Ogburn, M. B.:
23 The Impacts of Fisheries on Marine Ecosystems and the Transition to Ecosystem-Based
24 Management, *Annu. Rev. Ecol. Evol. Syst.*, 39, 259–278,
25 <https://doi.org/10.1146/annurev.ecolsys.39.110707.173406>, 2008.
- 26 Cullen, J. J.: Subsurface Chlorophyll Maximum Layers: Enduring Enigma or Mystery
27 Solved?, *Annu. Rev. Mar. Sci.*, 7, 207–239, <https://doi.org/10.1146/annurev-marine-010213-135111>, 2015.
- 29 Dall'Olmo, G. and Mork, K. A.: Carbon export by small particles in the Norwegian Sea,
30 *Geophys. Res. Lett.*, 41, 2921–2927, <https://doi.org/10.1002/2014GL059244>, 2014.
- 31 Doney, S. C., Lima, I., Moore, J. K., Lindsay, K., Behrenfeld, M. J., Westberry, T. K.,
32 Mahowald, N., Glover, D. M., and Takahashi, T.: Skill metrics for confronting global upper
33 ocean ecosystem-biogeochemistry models against field and remote sensing data, *J. Mar. Syst.*,
34 76, 95–112, <https://doi.org/10.1016/j.jmarsys.2008.05.015>, 2009.
- 35 D'Ortenzio, F. and d'Alcala, M. R.: On the trophic regimes of the Mediterranean Sea: a
36 satellite analysis, *Biogeosciences*, 6, 139–148, 2009.
- 37 Dutkiewicz, S., Hickman, A. E., Jahn, O., Gregg, W. W., Mouw, C. B., and Follows, M. J.:
38 Capturing optically important constituents and properties in a marine biogeochemical and
39 ecosystem model, *Biogeosciences*, 12, 4447–4481, <https://doi.org/10.5194/bg-12-4447-2015>,
40 2015.

- 1 Eriksen, M., Lebreton, L. C. M., Carson, H. S., Thiel, M., Moore, C. J., Borerro, J. C.,
2 Galgani, F., Ryan, P. G., and Reisser, J.: Plastic Pollution in the World's Oceans: More than 5
3 Trillion Plastic Pieces Weighing over 250,000 Tons Afloat at Sea, PLoS ONE, 9, e111913,
4 <https://doi.org/10.1371/journal.pone.0111913>, 2014.
- 5 European Union-Copernicus Marine Service: Global Ocean- In-Situ Near-Real-Time
6 Observations, <https://doi.org/10.48670/MOI-00036>, 2015.
- 7 European Union-Copernicus Marine Service: Global Ocean Biogeochemistry Analysis and
8 Forecast, <https://doi.org/10.48670/MOI-00015>, 2019.
- 9 European Union-Copernicus Marine Service: Global Ocean 3D Chlorophyll-a concentration,
10 Particulate Backscattering coefficient and Particulate Organic Carbon,
11 <https://doi.org/10.48670/MOI-00046>, 2020.
- 12 European Union-Copernicus Marine Service: Global Ocean Colour (Copernicus-GlobColour),
13 Bio-Geo-Chemical, L4 (monthly and interpolated) from Satellite Observations (Near Real
14 Time), <https://doi.org/10.48670/MOI-00279>, 2022.
- 15 Evers-King, H., Martinez-Vicente, V., Brewin, R. J. W., Dall'Olmo, G., Hickman, A. E.,
16 Jackson, T., Kostadinov, T. S., Krasemann, H., Loisel, H., Röttgers, R., Roy, S., Stramski, D.,
17 Thomalla, S., Platt, T., and Sathyendranath, S.: Validation and Intercomparison of Ocean
18 Color Algorithms for Estimating Particulate Organic Carbon in the Oceans, *Front. Mar. Sci.*,
19 4, 251, <https://doi.org/10.3389/fmars.2017.00251>, 2017.
- 20 Fay, A. R. and McKinley, G. A.: Global open-ocean biomes: mean and temporal variability,
21 *Earth Syst. Sci. Data*, 6, 273–284, <https://doi.org/10.5194/essd-6-273-2014>, 2014.
- 22 Fennel, K., Gehlen, M., Brasseur, P., Brown, C. W., Ciavatta, S., Cossarini, G., Crise, A.,
23 Edwards, C. A., Ford, D., Friedrichs, M. A. M., Gregoire, M., Jones, E., Kim, H.-C.,
24 Lamouroux, J., Murtugudde, R., Perruche, C., and the GODAE OceanView Marine
25 Ecosystem Analysis and Prediction Task Team: Advancing Marine Biogeochemical and
26 Ecosystem Reanalyses and Forecasts as Tools for Monitoring and Managing Ecosystem
27 Health, *Front. Mar. Sci.*, 6, 89, <https://doi.org/10.3389/fmars.2019.00089>, 2019.
- 28 Fennel, K., Mattern, J. P., Doney, S. C., Bopp, L., Moore, A. M., Wang, B., and Yu, L.:
29 Ocean biogeochemical modelling, *Nat. Rev. Methods Primer*, 2, 1–21,
30 <https://doi.org/10.1038/s43586-022-00154-2>, 2022.
- 31 Ford, D.: Assimilating synthetic Biogeochemical-Argo and ocean colour observations into a
32 global ocean model to inform observing system design, *Biogeosciences*, 18, 509–534,
33 <https://doi.org/10.5194/bg-18-509-2021>, 2021.
- 34 Friedlingstein, P., O'Sullivan, M., Jones, M. W., Andrew, R. M., Gregor, L., Hauck, J., Le
35 Quéré, C., Luijkx, I. T., Olsen, A., Peters, G. P., Peters, W., Pongratz, J., Schwingshackl, C.,
36 Sitch, S., Canadell, J. G., Ciais, P., Jackson, R. B., Alin, S. R., Alkama, R., Arneeth, A., Arora,
37 V. K., Bates, N. R., Becker, M., Bellouin, N., Bittig, H. C., Bopp, L., Chevallier, F., Chini, L.
38 P., Cronin, M., Evans, W., Falk, S., Feely, R. A., Gasser, T., Gehlen, M., Gkritzalis, T.,
39 Gloege, L., Grassi, G., Gruber, N., Gürses, Ö., Harris, I., Hefner, M., Houghton, R. A., Hurtt,
40 G. C., Iida, Y., Ilyina, T., Jain, A. K., Jersild, A., Kadono, K., Kato, E., Kennedy, D., Klein
41 Goldewijk, K., Knauer, J., Korsbakken, J. I., Landschützer, P., Lefèvre, N., Lindsay, K., Liu,

- 1 J., Liu, Z., Marland, G., Mayot, N., McGrath, M. J., Metzl, N., Monacci, N. M., Munro, D. R.,
2 Nakaoka, S.-I., Niwa, Y., O'Brien, K., Ono, T., Palmer, P. I., Pan, N., Pierrot, D., Pockock, K.,
3 Poulter, B., Resplandy, L., Robertson, E., Rödenbeck, C., Rodriguez, C., Rosan, T. M.,
4 Schwinger, J., Séférian, R., Shutler, J. D., Skjelvan, I., Steinhoff, T., Sun, Q., Sutton, A. J.,
5 Sweeney, C., Takao, S., Tanhua, T., Tans, P. P., Tian, X., Tian, H., Tilbrook, B., Tsujino, H.,
6 Tubiello, F., van der Werf, G. R., Walker, A. P., Wanninkhof, R., Whitehead, C., Willstrand
7 Wranne, A., et al.: Global Carbon Budget 2022, *Earth Syst. Sci. Data*, 14, 4811–4900,
8 <https://doi.org/10.5194/essd-14-4811-2022>, 2022.
- 9 Galí, M., Falls, M., Claustre, H., Aumont, O., and Bernardello, R.: Bridging the gaps between
10 particulate backscattering measurements and modeled particulate organic carbon in the ocean,
11 *Biogeochemistry: Open Ocean*, <https://doi.org/10.5194/bg-2021-201>, 2021.
- 12 Galí, M., Falls, M., Claustre, H., Aumont, O., and Bernardello, R.: Bridging the gaps between
13 particulate backscattering measurements and modeled particulate organic carbon in the ocean,
14 *Biogeosciences*, 19, 1245–1275, <https://doi.org/10.5194/bg-19-1245-2022>, 2022.
- 15 Garcia, H. E., Locarnini, R. A., Boyer, T. P., Antonov, J. I., Baranova, O. K., Zweng, M. M.,
16 Reagan, J. R., Johnson, D. R., Mishonov, A. V., and Levitus, S.: World ocean atlas 2013.
17 Volume 4, Dissolved inorganic nutrients (phosphate, nitrate, silicate), 2013.
- 18 Garcia, H. E., Boyer, T. P., Locarnini, R. A., Antonov, J. I., Mishonov, A. V., Baranova, O.
19 K., Zweng, M. M., Reagan, J. R., Johnson, D. R., and Levitus, S.: World ocean atlas 2013.
20 Volume 3, Dissolved oxygen, apparent oxygen utilization, and oxygen saturation, 2014.
- 21 Gasparin, F., Cravatte, S., Greiner, E., Perruche, C., Hamon, M., Van Gennip, S., and
22 Lellouche, J.-M.: Excessive productivity and heat content in tropical Pacific analyses:
23 Disentangling the effects of in situ and altimetry assimilation, *Ocean Model.*, 160, 101768,
24 <https://doi.org/10.1016/j.ocemod.2021.101768>, 2021.
- 25 Gehlen, M., Bopp, L., Emprin, N., Aumont, O., Heinze, C., and Ragueneau, O.: Reconciling
26 surface ocean productivity, export fluxes and sediment composition in a global
27 biogeochemical ocean model, *Biogeosciences*, 3, 521–537, [https://doi.org/10.5194/bg-3-521-](https://doi.org/10.5194/bg-3-521-2006)
28 2006, 2006.
- 29 Gehlen, M., Gangstø, R., Schneider, B., Bopp, L., Aumont, O., and Ethe, C.: The fate of
30 pelagic CaCO₃ production in a high CO₂ ocean: a model study, *Biogeosciences*, 4, 505–519,
31 <https://doi.org/10.5194/bg-4-505-2007>, 2007.
- 32 Gutknecht, E., Reffray, G., Mignot, A., Dabrowski, T., and Sotillo, M. G.: Modelling the
33 marine ecosystem of Iberia-Biscay-Ireland (IBI) European waters for CMEMS operational
34 applications, *Ocean Sci.*, 15, 1489–1516, <https://doi.org/10.5194/os-15-1489-2019>, 2019.
- 35 Hartigan, J. A. and Wong, M. A.: Algorithm AS 136: A K-Means Clustering Algorithm,
36 *Appl. Stat.*, 28, 100, <https://doi.org/10.2307/2346830>, 1979.
- 37 Hipsey, M. R., Gal, G., Arhonditsis, G. B., Carey, C. C., Elliott, J. A., Frassl, M. A., Janse, J.
38 H., de Mora, L., and Robson, B. J.: A system of metrics for the assessment and improvement
39 of aquatic ecosystem models, *Environ. Model. Softw.*, 128, 104697,
40 <https://doi.org/10.1016/j.envsoft.2020.104697>, 2020.

- 1 Iida, Y., Takatani, Y., Kojima, A., and Ishii, M.: Global trends of ocean CO₂ sink and ocean
2 acidification: an observation-based reconstruction of surface ocean inorganic carbon
3 variables, *J. Oceanogr.*, 1–36, 2020.
- 4 Johnson, Plant, J. N., Coletti, L. J., Jannasch, H. W., Sakamoto, C. M., Riser, S. C., Swift, D.
5 D., Williams, N. L., Boss, E., Haëntjens, N., Talley, L. D., and Sarmiento, J. L.:
6 Biogeochemical sensor performance in the SOCCOM profiling float array: SOCCOM
7 BIOGEOCHEMICAL SENSOR PERFORMANCE, *J. Geophys. Res. Oceans*, 122, 6416–
8 6436, <https://doi.org/10.1002/2017JC012838>, 2017.
- 9 Johnson, Plant, J. N., and Maurer, T. L.: Processing BGC-Argo pH data at the DAC level,
10 2018a.
- 11 Johnson, Pasquero De Fommervault, O., Serra, R., D’Ortenzio, F., Schmechtig, C., Claustre,
12 H., and Poteau, A.: Processing Bio-Argo nitrate concentration at the DAC Level, 2018b.
- 13 Key, R. M., Olsen, A., van Heuven, S., Lauvset, S. K., Velo, A., Lin, X., Schirnack, C.,
14 Kozyr, A., Tanhua, T., and Hoppema, M.: Global Ocean Data Analysis Project, Version 2
15 (GLODAPv2), Carbon Dioxide Information Analysis Center, Oak Ridge Nat Lab, 2015.
- 16 Kheireddine, M., Mayot, N., Ouhssain, M., and Jones, B. H.: Regionalization of the Red Sea
17 Based on Phytoplankton Phenology: A Satellite Analysis, *J. Geophys. Res. Oceans*, 126,
18 <https://doi.org/10.1029/2021JC017486>, 2021.
- 19 Lacour, L., Claustre, H., Prieur, L., and D’Ortenzio, F.: Phytoplankton biomass cycles in the
20 North Atlantic subpolar gyre: A similar mechanism for two different blooms in the Labrador
21 Sea: THE LABRADOR SEA BLOOMS, *Geophys. Res. Lett.*, 42, 5403–5410,
22 <https://doi.org/10.1002/2015GL064540>, 2015.
- 23 Landschützer, P., Gruber, N., Bakker, D. C. E., and Schuster, U.: Recent variability of the
24 global ocean carbon sink, *Glob. Biogeochem. Cycles*, 28, 927–949,
25 <https://doi.org/10.1002/2014GB004853>, 2014.
- 26 Lavigne, H., D’Ortenzio, F., Migon, C., Claustre, H., Testor, P., d’Alcalà, M. R., Lavezza, R.,
27 Houpert, L., and Prieur, L.: Enhancing the comprehension of mixed layer depth control on the
28 Mediterranean phytoplankton phenology: Mediterranean Phytoplankton Phenology, *J.*
29 *Geophys. Res. Oceans*, 118, 3416–3430, <https://doi.org/10.1002/jgrc.20251>, 2013.
- 30 Lazzari, Solidoro, C., Ibello, V., Salon, S., Teruzzi, A., Béranger, K., Colella, S., and Crise,
31 A.: Seasonal and inter-annual variability of plankton chlorophyll and primary production in
32 the Mediterranean Sea: a modelling approach, *Biogeosciences*, 9, 217–233,
33 <https://doi.org/10.5194/bg-9-217-2012>, 2012.
- 34 Lazzari, Solidoro, C., Salon, S., and Bolzon, G.: Spatial variability of phosphate and nitrate in
35 the Mediterranean Sea: A modeling approach, *Deep Sea Res. Part Oceanogr. Res. Pap.*, 108,
36 39–52, <https://doi.org/10.1016/j.dsr.2015.12.006>, 2016.
- 37 Lefèvre, N., Veeda, D., Tyaquicã, P., Perruche, C., Diverrès, D., and Ibánhez, J. S. P.: Basin-
38 Scale Estimate of the Sea-Air CO₂ Flux During the 2010 Warm Event in the Tropical North
39 Atlantic, *J. Geophys. Res. Biogeosciences*, 124, 973–986,
40 <https://doi.org/10.1029/2018JG004840>, 2019.

- 1 Lellouche, Greiner, E., Le Galloudec, O., Garric, G., Regnier, C., Drevillon, M., Benkiran,
2 M., Testut, C.-E., Bourdalle-Badie, R., Gasparin, F., Hernandez, O., Levier, B., Drillet, Y.,
3 Remy, E., and Le Traon, P.-Y.: Recent updates to the Copernicus Marine Service global
4 ocean monitoring and forecasting real-time 1/12° high-resolution system, *Ocean Sci.*, 14,
5 1093–1126, <https://doi.org/10.5194/os-14-1093-2018>, 2018.
- 6 Lellouche, J.-M., Le Galloudec, O., Drévillon, M., Régnier, C., Greiner, E., Garric, G., Ferry,
7 N., Desportes, C., Testut, C.-E., Bricaud, C., Bourdallé-Badie, R., Tranchant, B., Benkiran,
8 M., Drillet, Y., Daudin, A., and De Nicola, C.: Evaluation of global monitoring and
9 forecasting systems at Mercator Océan, *Ocean Sci.*, 9, 57–81, [https://doi.org/10.5194/os-9-57-](https://doi.org/10.5194/os-9-57-2013)
10 2013, 2013.
- 11 Letelier, R. M., Karl, D. M., Abbott, M. R., and Bidigare, R. R.: Light driven seasonal
12 patterns of chlorophyll and nitrate in the lower euphotic zone of the North Pacific
13 Subtropical Gyre, *Limnol. Oceanogr.*, 49, 508–519, 2004.
- 14 Long, M. C., Stephens, B. B., McKain, K., Sweeney, C., Keeling, R. F., Kort, E. A., Morgan,
15 E. J., Bent, J. D., Chandra, N., Chevallier, F., Commane, R., Daube, B. C., Krummel, P. B.,
16 Loh, Z., Luijkx, I. T., Munro, D., Patra, P., Peters, W., Ramonet, M., Rödenbeck, C., Stavert,
17 A., Tans, P., and Wofsy, S. C.: Strong Southern Ocean carbon uptake evident in airborne
18 observations, *Science*, 374, 1275–1280, <https://doi.org/10.1126/science.abi4355>, 2021.
- 19 Lynch, D. R., McGillicuddy, D. J., and Werner, F. E.: Skill assessment for coupled
20 biological/physical models of marine systems, *J. Mar. Syst.*, 1, 1–3, 2009.
- 21 Macías, D., Stips, A., and Garcia-Gorriz, E.: The relevance of deep chlorophyll maximum in
22 the open Mediterranean Sea evaluated through 3D hydrodynamic-biogeochemical coupled
23 simulations, *Ecol. Model.*, 281, 26–37, 2014.
- 24 Mayot, N., D’Ortenzio, F., Ribera d’Alcalà, M., Lavigne, H., and Claustre, H.: Interannual
25 variability of the Mediterranean trophic regimes from ocean color satellites, *Biogeosciences*,
26 13, 1901–1917, <https://doi.org/10.5194/bg-13-1901-2016>, 2016.
- 27 Mignot, Claustre, H., Uitz, J., Poteau, A., D’Ortenzio, F., and Xing, X.: Understanding the
28 seasonal dynamics of phytoplankton biomass and the deep chlorophyll maximum in
29 oligotrophic environments: A Bio-Argo float investigation, *Glob. Biogeochem. Cycles*, 28,
30 856–876, <https://doi.org/10.1002/2013GB004781>, 2014.
- 31 Mignot, A., Claustre, H., D’Ortenzio, F., Xing, X., Poteau, A., and Ras, J.: From the shape of
32 the vertical profile of in vivo fluorescence to Chlorophyll-a concentration, *Biogeosciences*,
33 8, 2391–2406, <https://doi.org/10.5194/bg-8-2391-2011>, 2011.
- 34 Mignot, A., D’Ortenzio, F., Taillandier, V., Cossarini, G., and Salon, S.: Quantifying
35 Observational Errors in Biogeochemical-Argo Oxygen, Nitrate, and Chlorophyll *a*
36 Concentrations, *Geophys. Res. Lett.*, 46, 4330–4337, <https://doi.org/10.1029/2018GL080541>,
37 2019.
- 38 Omand, M. M. and Mahadevan, A.: The shape of the oceanic nitracline, *Biogeosciences*, 12,
39 3273–3287, <https://doi.org/10.5194/bg-12-3273-2015>, 2015.

- 1 Osman, M. B., Das, S. B., Trusel, L. D., Evans, M. J., Fischer, H., Grieman, M. M., Kipfstuhl,
2 S., McConnell, J. R., and Saltzman, E. S.: Industrial-era decline in subarctic Atlantic
3 productivity, *Nature*, 569, 551–555, <https://doi.org/10.1038/s41586-019-1181-8>, 2019.
- 4 Park, J.-Y., Stock, C. A., Yang, X., Dunne, J. P., Rosati, A., John, J., and Zhang, S.: Modeling
5 Global Ocean Biogeochemistry With Physical Data Assimilation: A Pragmatic Solution to the
6 Equatorial Instability, *J. Adv. Model. Earth Syst.*, 10, 891–906,
7 <https://doi.org/10.1002/2017MS001223>, 2018.
- 8 Paulmier, A. and Ruiz-Pino, D.: Oxygen minimum zones (OMZs) in the modern ocean, *Prog.*
9 *Oceanogr.*, 80, 113–128, 2009.
- 10 Richardson, K. and Bendtsen, J.: Vertical distribution of phytoplankton and primary
11 production in relation to nutricline depth in the open ocean, *Mar. Ecol. Prog. Ser.*, 620, 33–46,
12 <https://doi.org/10.3354/meps12960>, 2019.
- 13 Rousseeuw, P. J.: Silhouettes: A graphical aid to the interpretation and validation of cluster
14 analysis, *J. Comput. Appl. Math.*, 20, 53–65, [https://doi.org/10.1016/0377-0427\(87\)90125-7](https://doi.org/10.1016/0377-0427(87)90125-7),
15 1987.
- 16 Roxy, M. K., Modi, A., Murtugudde, R., Valsala, V., Panickal, S., Prasanna Kumar, S.,
17 Ravichandran, M., Vichi, M., and Lévy, M.: A reduction in marine primary productivity
18 driven by rapid warming over the tropical Indian Ocean, *Geophys. Res. Lett.*, 43, 826–833,
19 <https://doi.org/10.1002/2015GL066979>, 2016.
- 20 Russell, J. L., Kamenkovich, I., Bitz, C., Ferrari, R., Gille, S. T., Goodman, P. J., Hallberg,
21 R., Johnson, K., Khazmutdinova, K., and Marinov, I.: Metrics for the evaluation of the
22 Southern Ocean in coupled climate models and earth system models, *J. Geophys. Res.*
23 *Oceans*, 123, 3120–3143, 2018.
- 24 Salon, S., Cossarini, G., Bolzon, G., Feudale, L., Lazzari, P., Teruzzi, A., Solidoro, C., and
25 Crise, A.: Novel metrics based on Biogeochemical Argo data to improve the model
26 uncertainty evaluation of the CMEMS Mediterranean marine ecosystem forecasts, *Ocean Sci.*,
27 15, 997–1022, <https://doi.org/10.5194/os-15-997-2019>, 2019.
- 28 Sauzède, R., Bittig, H. C., Claustre, H., Pasqueron de Fommervault, O., Gattuso, J.-P.,
29 Legendre, L., and Johnson, K. S.: Estimates of Water-Column Nutrient Concentrations and
30 Carbonate System Parameters in the Global Ocean: A Novel Approach Based on Neural
31 Networks, *Front. Mar. Sci.*, 4, <https://doi.org/10.3389/fmars.2017.00128>, 2017.
- 32 Schartau, M., Wallhead, P., Hemmings, J., Löptien, U., Kriest, I., Krishna, S., Ward, B. A.,
33 Slawig, T., and Oschlies, A.: Reviews and syntheses: parameter identification in marine
34 planktonic ecosystem modelling, *Biogeosciences*, 14, 1647–1701, [https://doi.org/10.5194/bg-](https://doi.org/10.5194/bg-14-1647-2017)
35 14-1647-2017, 2017.
- 36 Schmechtig, C., Poteau, A., Claustre, H., D’Ortenzio, F., and Boss, E.: Processing bio-Argo
37 chlorophyll-A concentration at the DAC level, *Ifremer*, <https://doi.org/10.13155/39468>, 2015.
- 38 Schmechtig, C., Claustre, H., Poteau, A., and D’Ortenzio, F.: Bio-Argo quality control
39 manual for the Chlorophyll-A concentration, *Ifremer*, <https://doi.org/10.13155/35385>, 2018.

- 1 Schmidt, H., Getzlaff, J., Löptien, U., and Oschlies, A.: Causes of uncertainties in the
2 representation of the Arabian Sea oxygen minimum zone in CMIP5 models, *Ocean Sci.*, 17,
3 1303–1320, <https://doi.org/10.5194/os-17-1303-2021>, 2021.
- 4 Schmidtko, S., Stramma, L., and Visbeck, M.: Decline in global oceanic oxygen content
5 during the past five decades, *Nature*, 542, 335–339, <https://doi.org/10.1038/nature21399>,
6 2017.
- 7 Schneider, B., Bopp, L., Gehlen, M., Segschneider, J., Frölicher, T. L., Cadule, P.,
8 Friedlingstein, P., Doney, S. C., Behrenfeld, M. J., and Joos, F.: Climate-induced interannual
9 variability of marine primary and export production in three global coupled climate carbon
10 cycle models, *Biogeosciences*, 5, 597–614, <https://doi.org/10.5194/bg-5-597-2008>, 2008.
- 11 Séférian, R., Bopp, L., Gehlen, M., Orr, J. C., Ethé, C., Cadule, P., Aumont, O., Salas y
12 Mélia, D., Voltaire, A., and Madec, G.: Skill assessment of three earth system models with
13 common marine biogeochemistry, *Clim. Dyn.*, 40, 2549–2573,
14 <https://doi.org/10.1007/s00382-012-1362-8>, 2013.
- 15 Solan, M., Archambault, P., Renaud, P. E., and März, C.: The changing Arctic Ocean:
16 consequences for biological communities, biogeochemical processes and ecosystem
17 functioning, *Philos. Trans. R. Soc. Math. Phys. Eng. Sci.*, 378, 20200266,
18 <https://doi.org/10.1098/rsta.2020.0266>, 2020.
- 19 Steinacher, M., Joos, F., Frölicher, T. L., Bopp, L., Cadule, P., Cocco, V., Doney, S. C.,
20 Gehlen, M., Lindsay, K., Moore, J. K., Schneider, B., and Segschneider, J.: Projected 21st
21 century decrease in marine productivity: a multi-model analysis, *Biogeosciences*, 7, 979–
22 1005, <https://doi.org/10.5194/bg-7-979-2010>, 2010.
- 23 Stow, C. A., Jolliff, J., McGillicuddy, D. J., Doney, S. C., Allen, J. I., Friedrichs, M. A. M.,
24 Rose, K. A., and Wallhead, P.: Skill assessment for coupled biological/physical models of
25 marine systems, *J. Mar. Syst.*, 76, 4–15, <https://doi.org/10.1016/j.jmarsys.2008.03.011>, 2009.
- 26 Stramma, L., Johnson, G. C., Sprintall, J., and Mohrholz, V.: Expanding Oxygen-Minimum
27 Zones in the Tropical Oceans, *Science*, 320, 655–658,
28 <https://doi.org/10.1126/science.1153847>, 2008.
- 29 Tagliabue, A., Bopp, L., Dutay, J.-C., Bowie, A. R., Chever, F., Jean-Baptiste, P., Bucciarelli,
30 E., Lannuzel, D., Remenyi, T., Sarthou, G., Aumont, O., Gehlen, M., and Jeandel, C.:
31 Hydrothermal contribution to the oceanic dissolved iron inventory, *Nat. Geosci.*, 3, 252–256,
32 <https://doi.org/10.1038/ngeo818>, 2010.
- 33 Terzić, E., Lazzari, P., Organelli, E., Solidoro, C., Salon, S., D’Ortenzio, F., and Conan, P.:
34 Merging bio-optical data from Biogeochemical-Argo floats and models in marine
35 biogeochemistry, *Biogeosciences*, 16, 2527–2542, <https://doi.org/10.5194/bg-16-2527-2019>,
36 2019.
- 37 Thierry, V. and Bittig, H.: Argo quality control manual for dissolved oxygen concentration,
38 2018.
- 39 Thierry, V., Bittig, H., Gilbert, D., Kobayashi, T., Kanako, S., and Schmid, C.: Processing
40 Argo oxygen data at the DAC level, Ifremer, <https://doi.org/10.13155/39795>, 2018.

- 1 Tuan Pham, D., Verron, J., and Christine Roubaud, M.: A singular evolutive extended
2 Kalman filter for data assimilation in oceanography, *J. Mar. Syst.*, 16, 323–340,
3 [https://doi.org/10.1016/S0924-7963\(97\)00109-7](https://doi.org/10.1016/S0924-7963(97)00109-7), 1998.
- 4 Tukey, J. W.: *Exploratory Data Analysis*, Addison-Wesley Publishing Company, 714 pp.,
5 1977.
- 6 Ward, B. A., Friedrichs, M. A. M., Anderson, T. R., and Oschlies, A.: Parameter optimisation
7 techniques and the problem of underdetermination in marine biogeochemical models, *J. Mar.*
8 *Syst.*, 81, 34–43, <https://doi.org/10.1016/j.jmarsys.2009.12.005>, 2010.
- 9 Westberry, T. K., Schultz, P., Behrenfeld, M. J., Dunne, J. P., Hiscock, M. R., Maritorea, S.,
10 Sarmiento, J. L., and Siegel, D. A.: Annual cycles of phytoplankton biomass in the subarctic
11 Atlantic and Pacific Ocean, *Glob. Biogeochem. Cycles*, 30, 175–190,
12 <https://doi.org/10.1002/2015GB005276>, 2016.
- 13 Williams, R. G. and Follows, M. J.: *Ocean dynamics and the carbon cycle: Principles and*
14 *mechanisms*, Cambridge University Press, 2011.
- 15 Wong, Keeley, Robert, Carval, Thierry, and Argo Data Management Team,: *Argo Quality*
16 *Control Manual for CTD and Trajectory Data*, <https://doi.org/10.13155/33951>, 2015.
- 17